Electronic supplementary information (ESI)

Shape-selective one-step synthesis of branched gold nanoparticles on the crystal surface of redox-active Pd^{II}-macrocycles

Yutaro Yamashita,[a] Shohei Tashiro,*[a] Yoshiki Ishii,[b] Takayuki Uchihashi,[b] Nobuyuki Matsushita,[c] Ryou Kubota[†a] and Mitsuhiko Shionoya*[a]

[a] Department of Chemistry, Graduate School of Science, The University of Tokyo, 7-3-1 Hongo, Bunkyo-ku, Tokyo 113-0033, Japan
[b] Department of Physics, Structural Biology Research Center, Graduate School of Science, Nagoya University, Furo-cho, Chikusa-ku, Nagoya, Aichi 464-8602, Japan
[c] Department of Chemistry, College of Science and Research Center for Smart Molecules, Rikkyo University, Nishi-Ikebukuro, Toshima-ku, Tokyo 171-8501, Japan
[†] Current address: Department of Synthetic Chemistry and Biological Chemistry, Graduate School of Engineering, Kyoto University, Katsura, Kyoto 615-8510, Japan

Table of contents

S1. Materials and methods

The macrocyclic tris(*o*-phenylenediamine) ligand **L** and millimeter-scale MMF single crystals were prepared according to our procedure.[1] $^{n}Bu_4N[AuCl_2]$ was prepared as described in a literature.[2] Solvents and reagents were purchased from TCI Co., Ltd., Kanto chemical Co., Inc. and FUJIFILM Wako Pure Chemical Corporation. All the chemicals were used without further purification. All the reactions were performed under aerobic conditions.

MMF is composed of four isomers of $Pd_3\mathbf{L}Cl_6$. The molar weight of a single complex ($Pd_3\mathbf{L}Cl_6$ = 1162.80) was basically used to calculate the molar mass and equivalent of MMF.

UV-visible absorption spectroscopy was performed using a JASCO V-770 spectrometer. Quartz cells of 1 cm or 0.1 cm were used for solution samples. For solid samples, diffuse reflectance was recorded at room temperature using an integrating sphere attachment, and the data were concerted to K-M function and normalized at 400 nm using JASCO's Spectra Manager, an integrated software package. Powder X-ray diffraction (PXRD) was recorded on a Rigaku XtaLAB P200 system diffractometer using CuKα radiation, and the obtained data were processed using the CrysAlisPro platform. Single-crystal X-ray crystallographic analyses were also carried out using a Rigaku XtaLAB P200 diffractometer with CuKα radiation, and the obtained data were analyzed using the Olex-2 crystallographic software package except for refinement[3] using SHELXL.[4] Scanning electron microscope (SEM) images and energy dispersive X-ray spectroscopy (EDS) data were obtained using a FEI Magellan 400L XHR. The size distributions of AuNPs were calculated using the equivalent diameters of the particles using ImageJ software. High-speed atomic force microscopy (HS-AFM) experiments were conducted using a laboratory-built apparatus.[5] Specifically, a miniaturized cantilever with a resonant frequency of 0.4–0.6 MHz, a quality factor of ~2 and a spring constant of ~0.1 N/m was used in solution, and the tapping mode was adopted as the operation mode. The amplitude of free oscillation of the cantilever was 2–3 nm, and the amplitude of the set point for feedback control at the sample surface was 60–80% of the free amplitude. All HS-AFM observations were carried out at room temperature. Transmission electron microscope (TEM) images and electron diffraction (ED) data were recorded on a JEOL JEM-2100F using copper micro grids (150 mesh). Zeta potentials were measured using Malvern Zetasizer Nano ZS with a disposal capillary cell (DTS1070). The nuclear magnetic resonance (NMR) spectra were measured using a Bruker AVANCE 500 spectrometer. NMR spectra were calibrated as below; CD_3CN: CHD_2CN = 1.94 ppm; DMSO-d_6: DMSO-d_5 = 2.50 ppm. Electrospray ionization-time-of-flight mass spectrometry (ESI-TOF-MS) measurements were conducted using a Waters LCT Premier XE spectrometer. X-ray fluorescence (XRF) was performed using a Rigaku NEX DE high-resolution energy dispersive spectrometer. Raman spectroscopy was carried out using a JASCO NRS-5100 micro-Raman spectrometer equipped with an optical density filter (O.D. = 3). A 785 nm laser and 20x lens were used.

S2. Shape-selective synthesis of AuNKs with MMF microcrystals

Preparation of MMF microcrystals

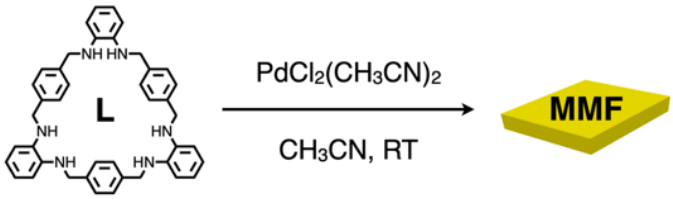

Experimental procedure: To a solution of **L** (24.8 mg, 39.3 μmol, 140 mL, 0.28 mM) in CH_3CN heated in water bath up to 70 °C, an acetonitrile solution of $PdCl_2(CH_3CN)_2$ (32.9 mg, 127 μmol, 3.23 eq, 6.35 mL, 20 mM) was added and stirred at room temperature for 15 h. The yellow precipitate was collected, washed well with CH_3CN and dried in vacuum to yield $Pd_3\mathbf{L}Cl_6\cdot(CH_3CN)_{0.11}\cdot(H_2O)_{6.52}$ (32.6 mg, 25.4 μmol, 65%). Millimeter-scale MMF single crystals were obtained by letting the combined CH_3CN solution stand at room temperature for one week.[1]

Elemental analysis: calcd for $C_{42}H_{42}Cl_6N_6Pd_3\cdot(CH_3CN)_{0.11}\cdot(H_2O)_{6.52}$: C 39.46%, H 4.35%, N 6.66%; found C 39.45%, H 4.26%, N 6.65%.

The ^{1}H NMR spectrum of the dried sample in DMSO-d_6 was consistent with that of the reported $Pd_3\mathbf{L}Cl_6$[1] (Fig. S1). DCl-DMSO-d_6 (0.1 M) was used to dissociate the coordination bonds of $Pd_3\mathbf{L}Cl_6$ and the molar ratio of ligand **L** to CH_3CN was estimated to calculate the number of solvent molecules contained. The calculated molar ratio, **L**/CH_3CN = 1:0.11, was in agreement with the result of elemental analysis.

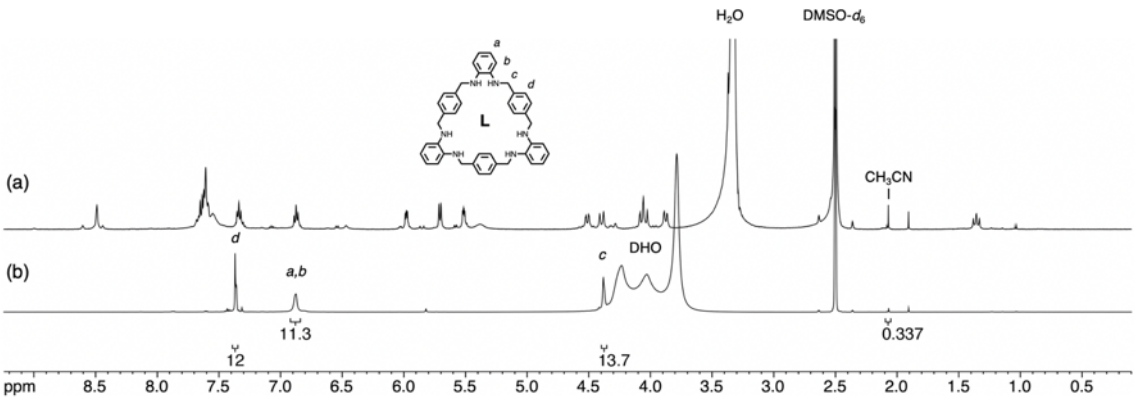

Fig. S1 ^{1}H NMR spectra (500 MHz, 300 K) of the components of MMF. (a) MMF dissolved in DMSO-d_6. (b) MMF dissolved in DCl-DMSO-d_6.

The PXRD pattern of MMF microcrystals immersed in CH_3CN was in good agreement with the calculated pattern, but the dried sample lost their crystallinity (Fig. S2). However, when the dried MMF was immersed in CH_3CN again, the crystallinity was recovered.

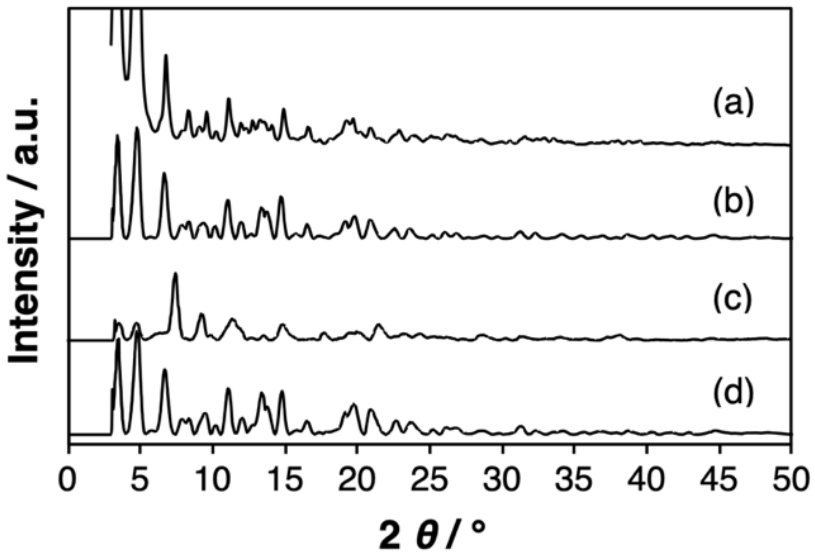

Fig. S2 Powder X-ray diffraction patterns (20 °C) of MMF. (a) MMF simulated from the single-crystal structure. As-synthesized microcrystalline MMF (b) soaked in CH_3CN, (c) dried in vacuum and (d) re-soaked in CH_3CN after drying in vacuum.

The microscopic shape of the product was similar to that of rhombic MMF single crystals[1] (Fig. S3).

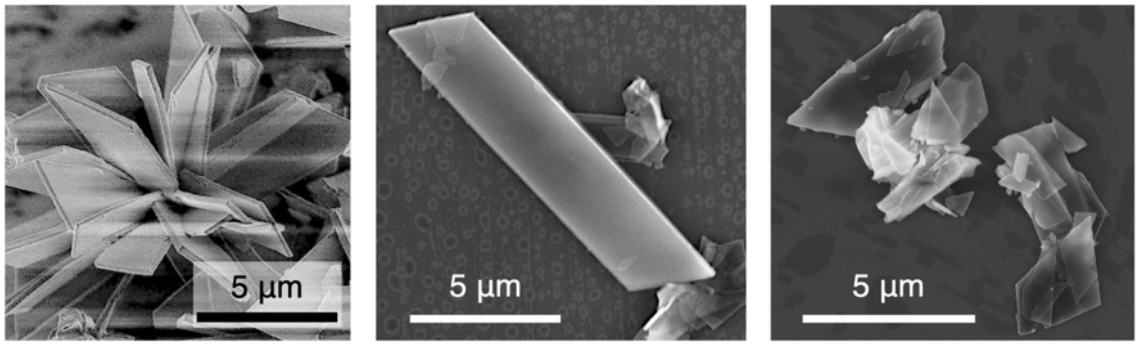

Fig. S3 Representative SEM images of MMF microcrystals. Measurement conditions: 1.00 kV, 6.3 pA for the left image; 15.00 kV, 0.20 nA for the center image; 5.00 kV, 50 pA for the right image.

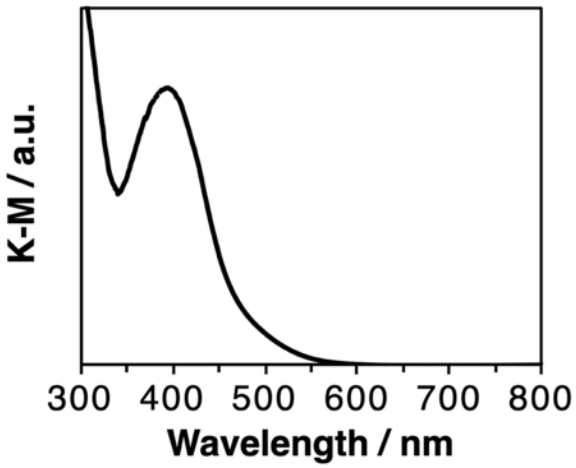

Fig. S4 Solid-state absorption (Kubelka-Munk function) spectrum of MMF microcrystals.

Typical procedure for the shape-selective one-step synthesis of AuNK/MMF with L-Asc/$HAuCl_4$ = 100:1

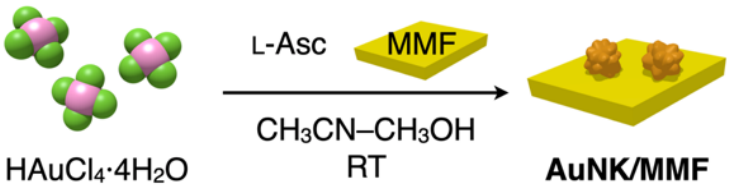

Experimental procedure: MMF microcrystals (0.50 mg, 0.43 μmol, 0.80 eq) were dispersed into a solution of $HAuCl_4 \cdot 4H_2O$ (0.50 mM, 1.1 mL, 0.54 μmol) in CH_3CN and added to a solution of L-ascorbic acid (L-Asc, 0.20 M, 0.27 mL, 54 μmol, 100 eq) in CH_3OH. After stirring min at room temperature for 30, the brown solid was collected, washed with CH_3OH, and dried in air.

Quantitative analysis of AuNK/MMF

Sample preparation: AuNK/MMF was synthesized in two batches according to the typical experimental procedure described above (Table S1). The products were collected and combined for elemental analysis. The samples for X-ray fluorescence (XRF) were also prepared by the same procedure.

Elemental analysis: calcd for $C_{42}H_{42}Cl_6N_6Pd_3Au_{0.74} \cdot (H_2O)_{13.76}$: C 32.40%, H 4.51%, N 5.40%; found C 32.37%, H 4.35%, N 5.41%.

XRF: Pd/Au = 3.00:0.744.

Table S1 Amount of MMF, $HAuCl_4 \cdot 4H_2O$, and L-Asc used in the syntheses of AuNKs and the amount of produced AuNK/MMF.

#	MMF / mg	MMF / μmol	$HAuCl_4 \cdot 4H_2O$ / μmol	L-Asc / μmol	AuNK/MMF / mg
1	2.51	1.95	2.70	270	2.08
2	2.48	1.93	2.66	266	2.05
Total	4.99	3.88	5.36	536	4.13

The result of elemental analysis agreed with that of XRF. Concluding these results, the yield of Au and the lost amount of MMF crystals were calculated as shown in Table S2. The yield of Au obtained as AuNKs was estimated to be 37%. The yield of MMF, 58%, means that 42% (1.25 mg, 0.97 μmol) of the MMF crystals had been lost by dissolution in the reaction solution probably due to the strong acidity of $HAuCl_4$ or redox reactions with Au. Since the amounts of reduced Au (2.0 μmol) and lost MMF (0.97 μmol) are comparable, it is likely that MMF reduced Au^I stoichiometrically rather than as a catalyst, and MMF that was not involved in the reduction reaction remained in the crystal.

Table S2 Amounts and yields of MMF and Au calculated from the results of elemental analysis and XRF.

	Used / mg	Used / μmol	Obtained / mg	Obtained / μmol	Yield / %
MMF	4.99	3.88	3.74	2.91	58
Au		5.36	0.39	2.0	37

Reaction tracking on the synthesis of AuNK/MMF by UV-vis absorption spectroscopy

Experimental procedure: MMF microcrystals (0.66 mg, 0.57 μmol, 0.80 eq) were stirred with a solution of $HAuCl_4 \cdot 4H_2O$ (0.40 mM, 0.71 μmol) and L-Asc (40 mM, 71 μmol, 100 eq) in CH_3CN–CH_3OH (4:1 v/v) min at room temperature for 30. After the reaction, the supernatant solution was sampled by centrifugation and filtration.

After 30 min, the absorption band at 325 nm characteristic of $HAuCl_4$ was reduced because Au^{III} was reduced to Au^0 in two steps via Au^I (Fig. S5). On the other hand, a broad small shoulder was observed around 400 nm, which indicates that MMF dissolved as $Pd_3\mathbf{L}Cl_6$ or its oxidized form.

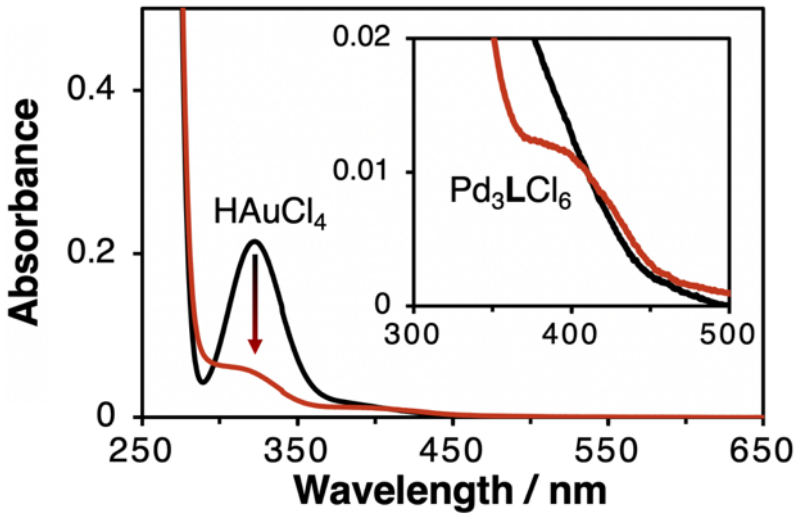

Fig. S5 Absorption spectra (20 °C) at the beginning (black) and after 30 min (red) of the supernatant solution of $HAuCl_4 \cdot 4H_2O$ and L-Asc dissolved in CH_3CN–CH_3OH (4:1 v/v) containing MMF.

Size controlled synthesis of AuNKs

AuNK synthesis with L-Asc/$HAuCl_4$ = 250:1: MMF microcrystals (0.42 mg, 0.36 μmol, 0.0020 eq) were dispersed into a solution of $HAuCl_4 \cdot 4H_2O$ (0.20 mM, 0.90 mL, 0.18 mmol) in CH_3CN and added to a solution of L-Asc (0.20 M, 0.23 mL, 46 mmol, 250 eq) in CH_3OH. After stirring at room temperature for 30 min, the beige solid components were collected, washed with CH_3OH, and dried in air.

AuNK synthesis with L-Asc/$HAuCl_4$ = 1000:1: MMF microcrystals (0.43 mg, 0.37 μmol, 0.0080 eq) were dispersed into an acetonitrile solution of $HAuCl_4 \cdot 4H_2O$ (0.050 mM, 0.92 mL, 46 μmol) and added to a solution of L-Asc (0.20 M, 0.23 mL, 46 mmol, 1000 eq) in CH_3OH. After stirring for 30 min at room temperature, the beige solid components were collected, washed with CH_3OH, and dried in air.

AuNK synthesis with L-Asc/$HAuCl_4$ = 2500:1: MMF microcrystals (0.38 mg, 0.33 μmol, 0.021 eq) were dispersed into a solution of $HAuCl_4 \cdot 4H_2O$ (0.020 mM, 0.82 mL, 16 nmol) in CH_3CN and added to a solution of L-Asc (0.20 M, 0.20 mL, 40 μmol, 2500 eq) in CH_3OH. After stirring at room temperature for 30 min, the dark yellow solid components were collected, washed with CH_3OH, and dried in air.

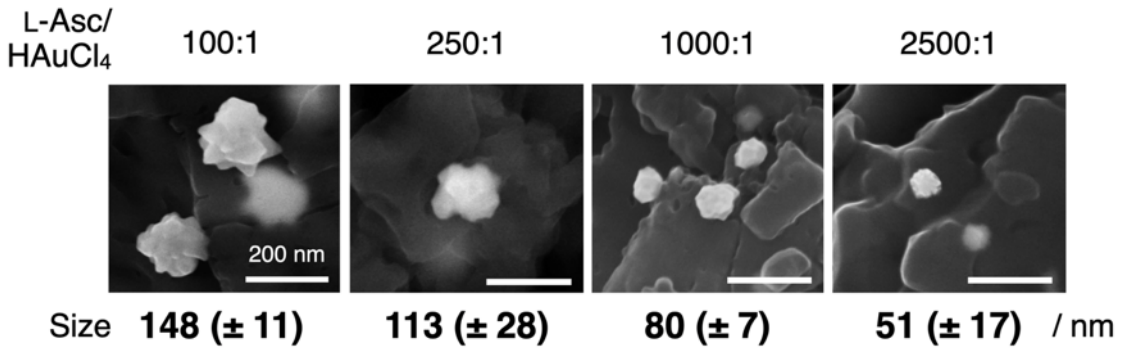

Fig. S6 Representative SEM images of AuNKs (15.00 kV, 0.20 nA) deposited on MMF microcrystals synthesized by varying the ratios of L-Asc/$HAuCl_4$.

Isolation of AuNKs

Experimental procedure: As-synthesized AuNK/MMF (1.9 mg) was dissolved in 0.8 mL of DMSO and collected by centrifugation. The precipitate was further washed with DMSO (0.8 mL) and CH_3OH (0.5 mL, three times) by centrifugation and dried in vacuo to obtain a dark brown solid (0.32 mg). For absorption spectroscopy, the solid was dispersed into 700 μL of water.

Thermal stability of AuNKs

Experimental procedure: As-synthesized AuNK/MMF (1.99 mg) was dissolved in 0.8 mL of DMSO and collected by centrifugation. The precipitate was further washed with DMSO (0.8 mL) and CH_3OH (0.5 mL, three times) by centrifugation and dried in vacuo to give a dark brown solid (0.41 mg). The solid was redispersed in H_2O (0.8 mL) and stirred at 50 °C for 30 min.

The SEM images before and after heating showed that the shape and size of AuNK seemed to be maintained, suggesting the thermal stability of AuNKs in H_2O (Fig. S7).

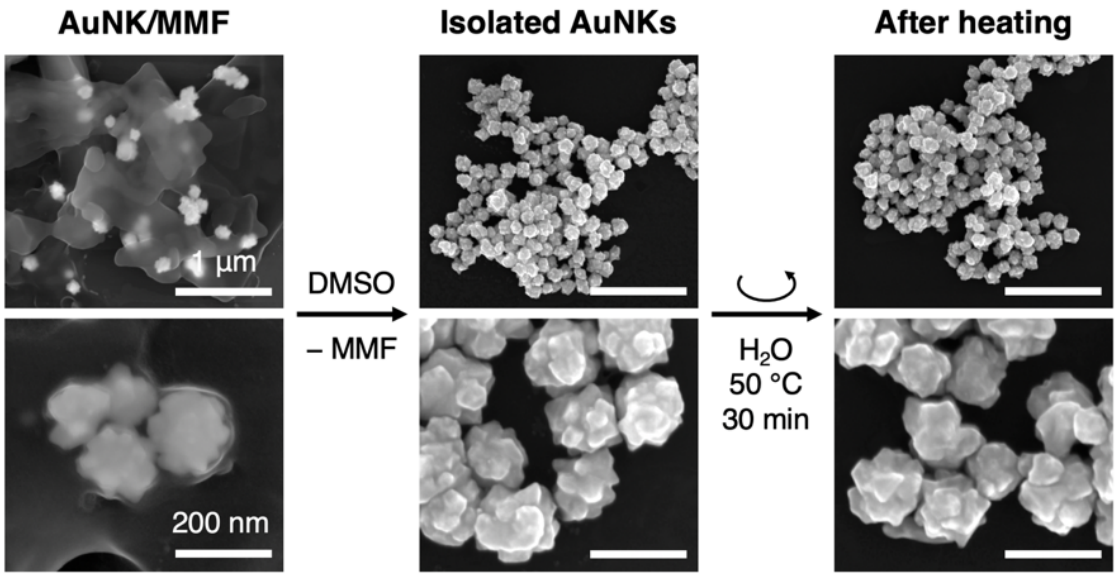

Fig. S7 Representative SEM images (15.00 kV, 0.20 nA) of AuNK/MMF and the isolated AuNKs before and after heating in H_2O at 50 °C.

S3. Reduction of Au^{I} by MMF

Reduction of $HAuCl_4$ in the presence and absence of MMF

Experimental procedure: A solution of $HAuCl_4 \cdot 4H_2O$ (0.40 mM, 1.0 μmol) and L-Asc (40 mM, 100 μmol, 100 eq) in CH_3CN–CH_3OH (4:1 v/v) was stirred for 5 h. To MMF microcrystals (0.70 mg, 0.60 μmol), 1.7 mL of the resultant colorless solution was added and further stirred for 30 min. The resulting brown suspension was centrifuged to separate the supernatant from the precipitate, which was washed with CH_3OH and dried in air. The supernatant solution was filtered and subjected to UV-vis absorption spectroscopy.

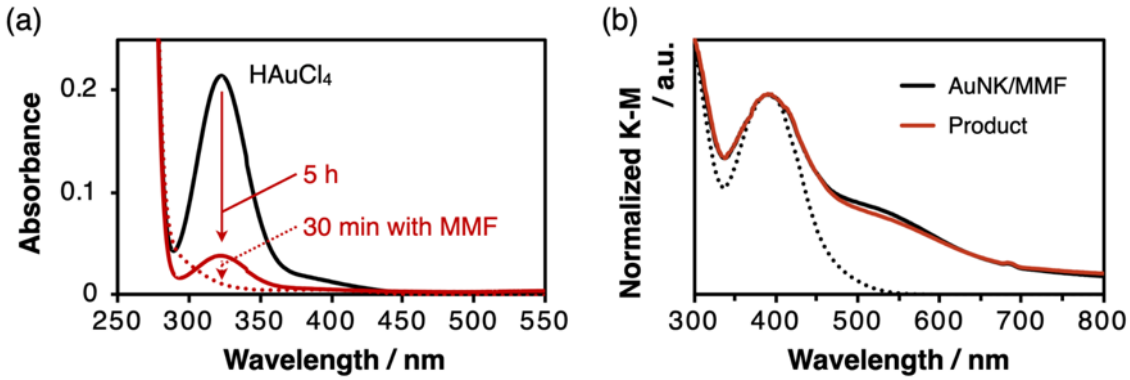

Fig. S8 Absorption spectra in the reduction of $HAuCl_4$ in the presence and absence of MMF. (a) Absorption spectra at 20 °C, at the beginning (black) and after 5 h (red solid line), of the supernatant solution containing $HAuCl_4 \cdot 4H_2O$ and L-Asc in CH_3CN–CH_3OH (4:1, v/v) without MMF. The red dotted line shows the spectrum of the supernatant solution after subsequent addition of MMF and stirring for another 30 min. (b) Solid-state absorption spectra (Kubelka-Munk function, rt) of as-synthesized MMF (dotted black line), standard AuNK/MMF (black solid line) and the product obtained by mixing the colorless Au^{I} solution and MMF (solid red line).

Reduction of $^{n}Bu_4N[AuCl_2]$ with MMF

Experimental procedure: To a solution of $^{n}Bu_4N[AuCl_2]$ (0.50 mM, 1.7 mL, 0.83 μmol) in CH_3CN, MMF microcrystals (0.77 mg, 0.66 μmol, 0.80 eq) were added and stirred at room temperature for 30 min. The resulting solid components were collected, washed with acetonitrile, and dried in air.

The absorption spectrum after the reaction showed a broad shoulder around 550 nm (Fig. S9), which corresponds to the surface plasmon band of AuNPs. By SEM observation of the surface (Fig.

S10), AuNPs with an average size of 30 nm were found on MMF microcrystals.

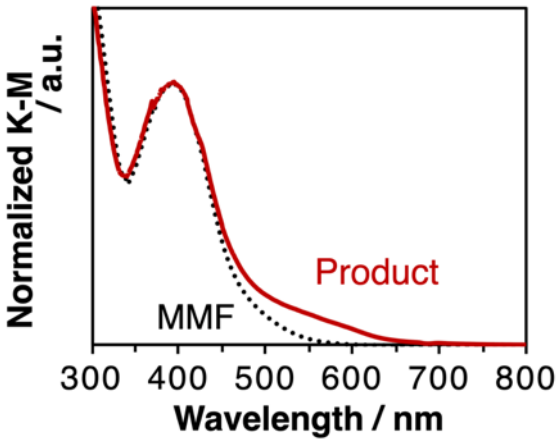

Fig. S9 Solid-state absorption (Kubelka-Munk function) spectra of MMF before (black dotted line) and after (red solid line) the reaction with $^{n}Bu_4N[AuCl_2]$.

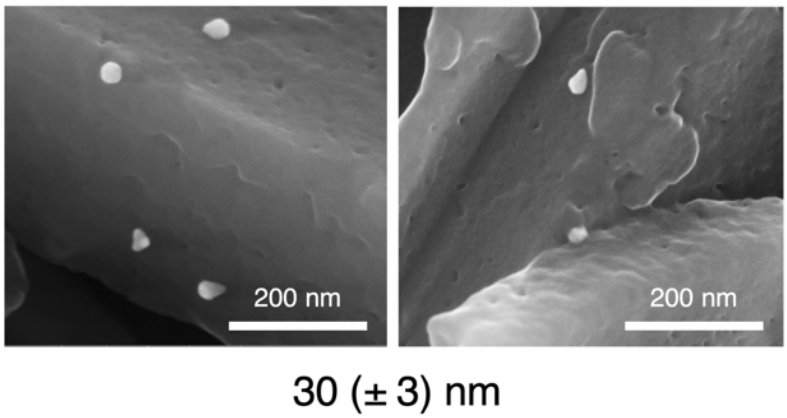

Fig. S10 Representative SEM images (15.00 kV, 0.20 nA) of MMF microcrystals after the reaction with $^{n}Bu_4N[AuCl_2]$.

Mixing of $HAuCl_4$ with MMF

Experimental procedure: MMF microcrystals (0.76 mg, 0.65 μmol, 0.79 eq) were stirred with a solution of $HAuCl_4 \cdot 4H_2O$ (0.50 mM, 0.82 μmol) in CH_3CN at room temperature for 30 min. Before and after the reaction, aliquots of the supernatant solution were sampled, filtered and UV-vis absorption spectra were measured.

Immediately after mixing $HAuCl_4 \cdot 4H_2O$ with MMF, a slight increase in absorbance was observed in some wavelength regions, and the increase with time was attributed to the dissolution of MMF as $Pd_3\mathbf{L}Cl_6$ (Fig. S11). However, there was no decrease in the characteristic absorption band of $HAuCl_4$,

indicating that MMF did not reduce Au^{III}.

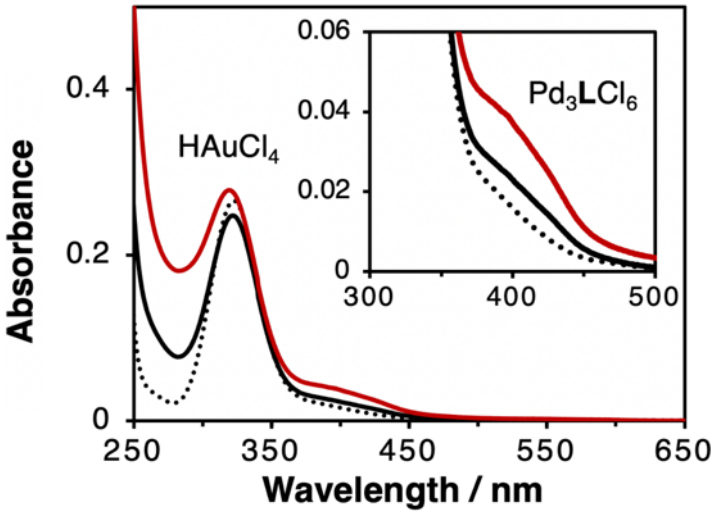

Fig. S11 Absorption spectra (20 °C) in the reaction of $HAuCl_4 \cdot 4H_2O$ with MMF. Black dotted line: $HAuCl_4 \cdot 4H_2O$ only. Solid lines: the acetonitrile supernatant solution of $HAuCl_4 \cdot 4H_2O$ and MMF at the beginning (black) and after 30 min (red).

Reaction in CH_3CN–CH_3OH without L-Asc

Experimental procedure: MMF microcrystals (0.57 mg, 0.49 μmol, 0.80 eq) were dispersed in a CH_3CN solution of $HAuCl_4 \cdot 4H_2O$ (0.50 mM, 1.2 mL, 0.61 μmol) and added to CH_3OH (0.31 mL). After stirring at room temperature for 30 min, the dark yellow solid was collected, washed with CH_3OH, and dried in air.

The solid-state absorption spectrum after the reaction of $HAu^{III}Cl_4$ with MMF in the absence of L-Asc showed a small shoulder around 520 nm (Fig. S12). This indicates that small amount of AuNPs were formed despite the absence of L-Asc. As shown in Fig. 4 in the main text, CH_3OH does not reduce Au^I, suggesting that CH_3OH acts as a reducing agent from Au^{III} to Au^I, and further reduction to Au^0 occurs by MMF. Since the increase in absorbance is much smaller than that of AuNK/MMF, it is possible that the reducing agent from Au^{III} to Au^I in the synthesis of AuNKs is mainly L-Asc, but CH_3OH may also contribute.

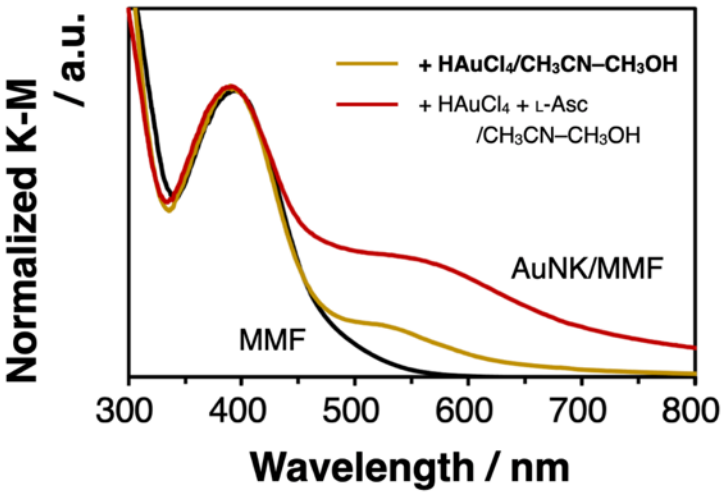

Fig. S12 Solid-state absorption (Kubelka-Munk function) spectra of MMF microcrystals. MMF before reaction (black), after stirring with $HAuCl_4 \cdot 4H_2O$ in $CH_3CN–CH_3OH$ (4:1 v/v) (yellow) and standard AuNK/MMF obtained by reaction of $HAuCl_4 \cdot 4H_2O$ with L-Asc in $CH_3CN–CH_3OH$ (red).

Reduction of ^{n}Bu$_4$N[AuCl$_2$] with Pd$_3$LCl$_6$

Analysis by UV-vis absorption spectroscopy: Acetonitrile solutions of **L** (0.28 mM, 3.7 mL, 1.0 μmol) and $PdCl_2(CH_3CN)_2$ (20 mM, 0.17 mL, 3.3 μmol, 3.3 eq) were mixed and left at room temperature for 1 h. After filtration, 1.8 mL (0.48 μmol of Pd_3**L**Cl_6) of the yellow solution was added to a solution of ^{n}Bu$_4$N[AuCl$_2$] (0.76 mM, 0.81 mL, 0.62 μmol, 1.2 eq) in CH_3CN and stirred at room temperature for 3 h. The aliquots of the reaction suspension after filtration were sampled for UV-vis absorption spectroscopy. The resulting yellow solid components were collected by filtration, washed with CH_3CN and dried in air.

During the reaction, the inner wall of the reaction tube was colored pinkish, which indicated the formation of AuNPs. After the reaction, a yellow precipitate of *in-situ* crystallized MMF was observed. The solid-state absorption spectrum of the precipitate had a small but broad shoulder around 550 nm, suggesting the presence of AuNPs (Fig. S13).

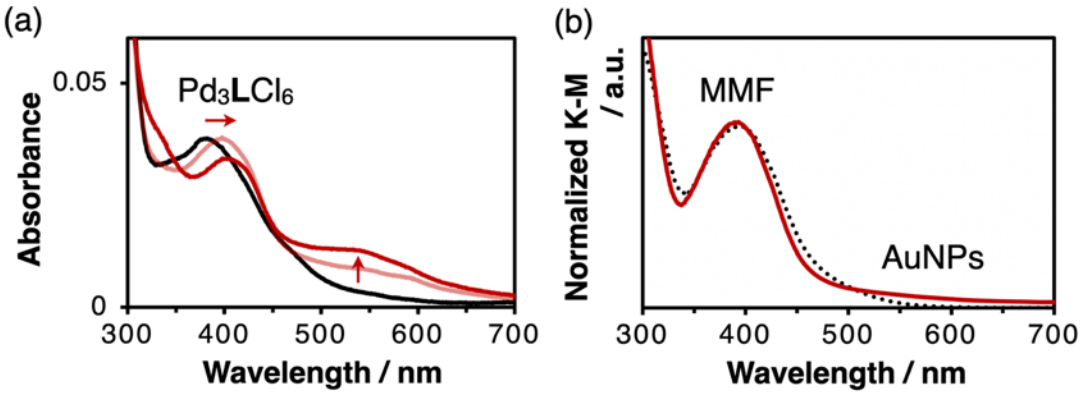

Fig. S13 Absorption spectra in the reduction of $^{n}Bu_4N[AuCl_2]$ by $Pd_3\mathbf{L}Cl_6$. (a) Absorption spectra at 20 °C of the supernatant solution of $^{n}Bu_4N[AuCl_2]$ and $Pd_3\mathbf{L}Cl_6$ in CH_3CN at the beginning (black), after 1 h (pink) and 3 h (red). (b) Solid-state absorption (Kubelka-Munk function) spectra of as-synthesized MMF (black dotted line) and the product obtained from the reaction between $^{n}Bu_4N[AuCl_2]$ and $Pd_3\mathbf{L}Cl_6$ (red solid line).

Analysis by ESI-MS: Acetonitrile solutions of $Pd_3\mathbf{L}Cl_6$ and $^{n}Bu_4N[AuCl_2]$ prepared in the above-mentioned way were mixed and the supernatant solution after 3 h was examined by ESI-TOF-MS (Figs. S14 and S15).

The mass spectra showed isotope patterns derived from $Pd_3\mathbf{L}Cl_6$ and various adducts in both positive and negative modes, regardless of whether the reaction with $^{n}Bu_4N[AuCl_2]$ was before or after. On the other hand, unidentified minor signals were also observed in both spectra. One of them ($m/z \approx$ 1152 in Fig. S12b) had an isotope pattern similar to that of $H_{-12}Pd_3\mathbf{L}Cl_6$, the fully oxidized form of $Pd_3\mathbf{L}Cl_6$, although it was not a perfect match.

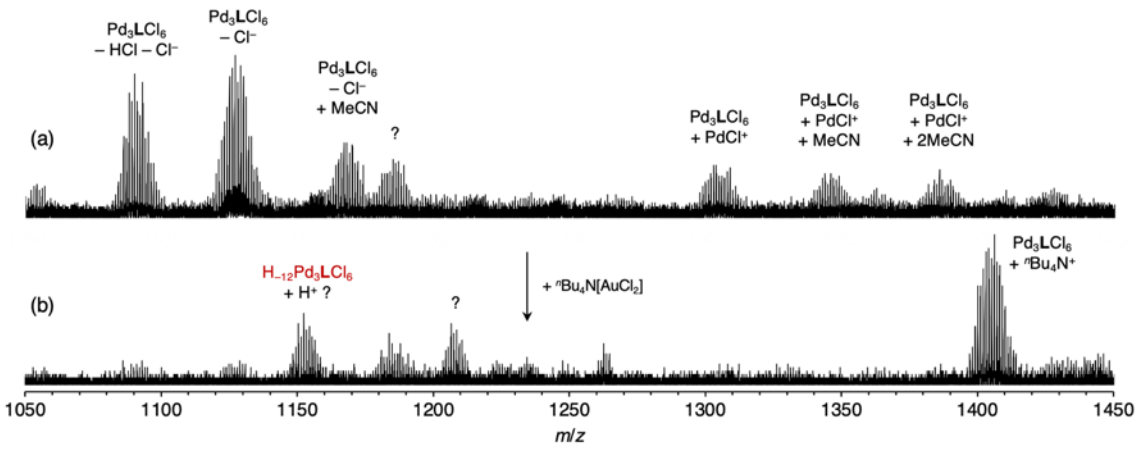

Fig. S14 ESI-TOF-MS spectra (Positive, CH_3CN). (a) Pd_3**L**Cl_6 4 h after mixing **L** and $PdCl_2(CH_3CN)_2$. (b) Pd_3**L**Cl_6 in the presence of 1.25 eq of ^{n}$Bu_4N[AuCl_2]$.

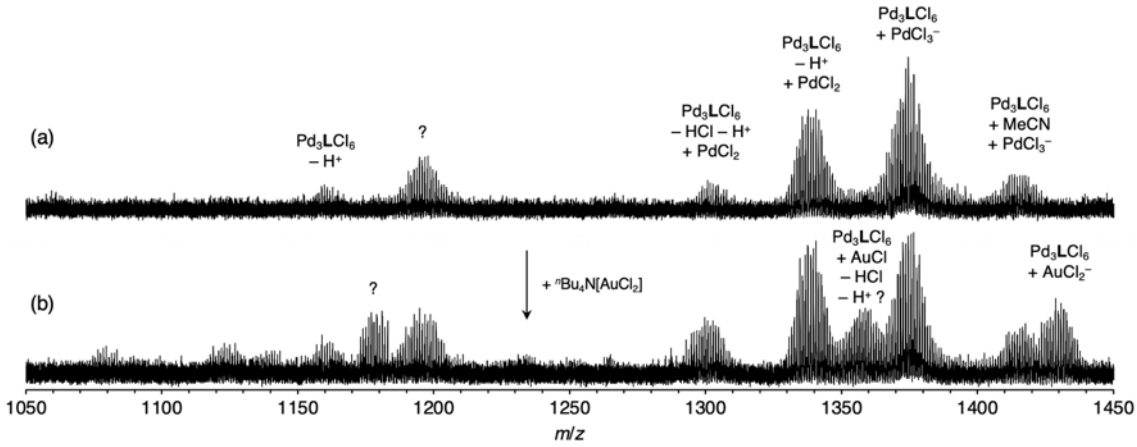

Fig. S15 ESI-TOF-MS spectra (Negative, CH_3CN). (a) Pd_3**L**Cl_6 4 h after mixing **L** and $PdCl_2(CH_3CN)_2$. (b) Pd_3**L**Cl_6 in the presence of 1.25 eq of ^{n}$Bu_4N[AuCl_2]$.

Analysis by ^{1}H NMR: Solutions of **L** (0.28 mM, 0.80 mL, 0.22 μmol) and $PdCl_2(CH_3CN)_2$ (18 mM, 40 μL, 0.73 μmol, 3.3 eq) in CD_3CN were mixed and left at room temperature for 2 h. To the mixture, ^{n}$Bu_4N[AuCl_2]$ (0.17 mg, 0.33 μmol, 1.5 eq) was added and left at room temperature for 3 h and then examined by ^{1}H NMR (Fig. S16).

The NMR signals of Pd_3**L**Cl_6 in the aromatic region were broad and unclear due to mainly the fast inversion of the *anti*-isomers. Furthermore, the signal intensity decreased over time due to the precipitation of MMF crystals, making it difficult to detect changes in the complexes.

In conclusion, it was difficult to identify the oxidized products of Pd_3**L**Cl_6 by mass spectrometry and NMR spectroscopy. Therefore, we tried to estimate the possible structures of the oxidized products by DFT calculations using mononuclear Pd(II) complexes as simple models.

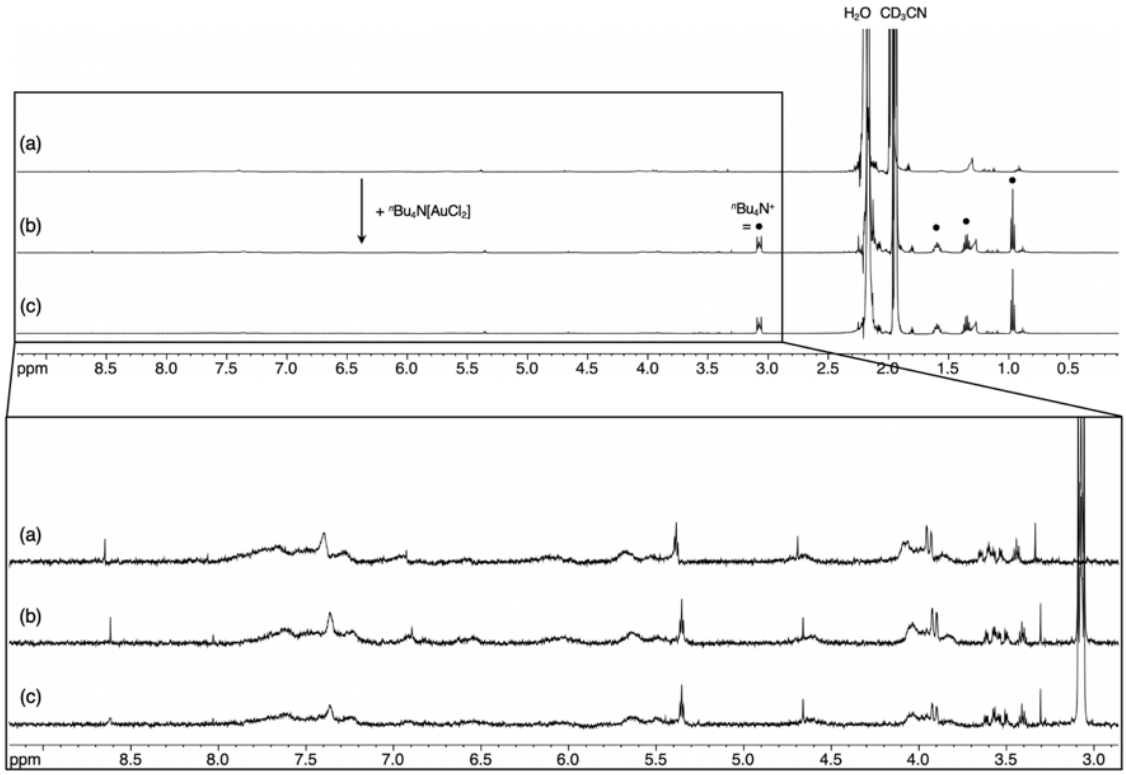

Fig. S16 ^{1}H NMR spectra (CD_3CN, 500 MHz, 300 K). (a) Pd_3**L**Cl_6 2 h after mixing **L** and $PdCl_2(CH_3CN)_2$. (b) (a) in the presence of 1.5 eq of ^{n}Bu$_4$N[$AuCl_2$]. (c) (b) after 3 h at room temperature.

Electrochemical property

As a supplementary experiment, cyclic voltammetry was preliminarily performed for CH_3CN solutions of Pd_3**L**Cl_6 and ^{n}Bu$_4$N[$AuCl_2$]. However, both showed complex redox waves that were difficult to assign properly. The complex spectra may be due to the multi-step reaction of the three non-innocent phenylenediamine ligands of Pd_3**L**Cl_6,[6] the redox reaction of the Pd center, the redox reactions of both complexes with chloride ions, and the irreversible deposition and dissolution of Au.[7–9]

Therefore, there are several possible reduction mechanisms of Au^I, such as disproportionation, electron transfer due to the interactions between Pd_3**L**Cl_6 and ^{n}Bu$_4$N[$AuCl_2$], and the redox reactions due to deprotonation from Pd_3**L**Cl_6. Of these, the redox reactions involving them are partly supported by the experimental results and theoretical calculations, as described below.

DFT calculation using model complexes

The UV-vis absorption spectra of the model complexes **S1**–**S5** shown in Fig. S17 were simulated using time-dependent density functional theory (TD-DFT) calculations. **S1** is a partial structure of Pd_3**L**Cl_6, and **S2** is a dianionic form without two protons in the amine groups. **S3** and **S4** are oxidized products from which one or two electrons have been removed from **S2**, respectively. **S5** is another oxidized product of **S2** with two hydrogens removed from the benzylic and amine groups.

First, the ground states of **S1**–**S5** were optimized by DFT calculations using B3LYP functional[10] (Fig. S18). The relativistic effective core potential (RECP) with LANL2DZ basis sets was used for Pd atoms, and 6-31+G(d) was used for C, H, N and Cl atoms.[11] The Cartesian coordinates of the optimized structures for **S1**–**S5** are shown at the end of this document.

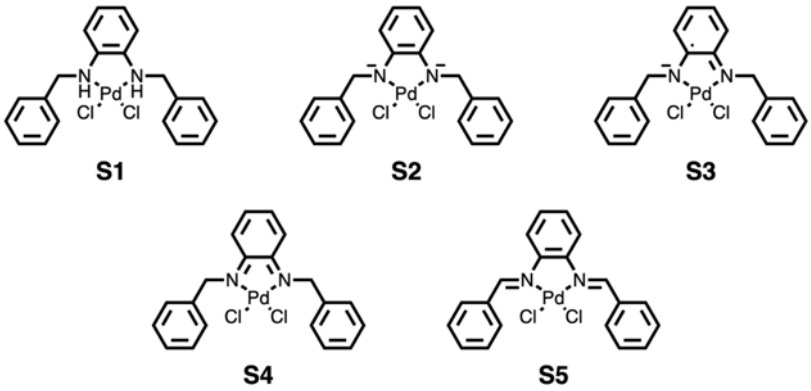

Fig. S17 Model complexes used in the DFT calculations.

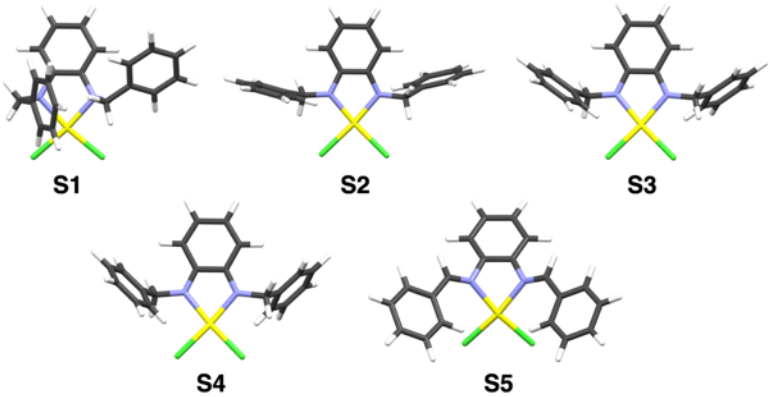

Fig. S18 Optimized structures of the model complexes.

Next, the UV-vis spectra of **S1**–**S5** were optimized by TD-DFT calculations using B3LYP functional. The RECP with LANL2DZ basis sets was used for Pd atoms, and 6-31+G(d) was used for C, H, N and Cl atoms. Twenty excitation modes were calculated from low frequency (Fig. S19).

The excitations of **S1** at 379.50 nm (Oscillator strength f = 0.0094) and **S5** at 416.14 nm (f = 0.0379) are most likely the cause of the red shift around 400 nm as shown in Fig. S11a. Both of these two excitations are associated with transitions to a Pd–Cl σ* orbitals, as shown in Fig. S20. On the other hand, the characteristic excitations of oxidized species **S3** and **S4** at 500–600 nm are consistent with the broad shoulder around 550 nm, as shown in Fig. S13a. Absorption in this wavelength range is common to the radical species of non-innocent Pd^{II}–phenylenediamine complexes reported in literatures.[6]

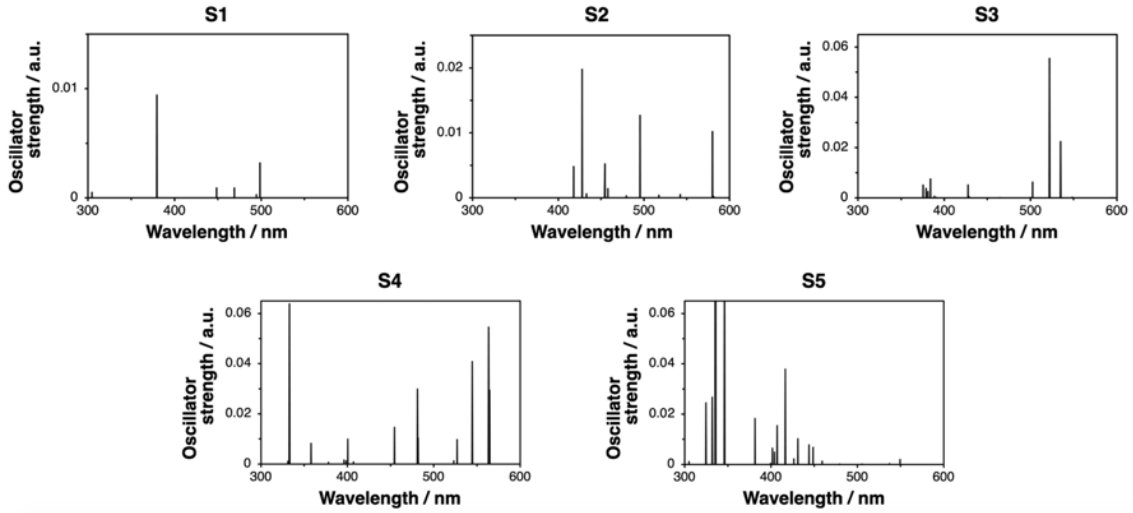

Fig. S19 Simulated absorption spectra of the model complexes S1–S5.

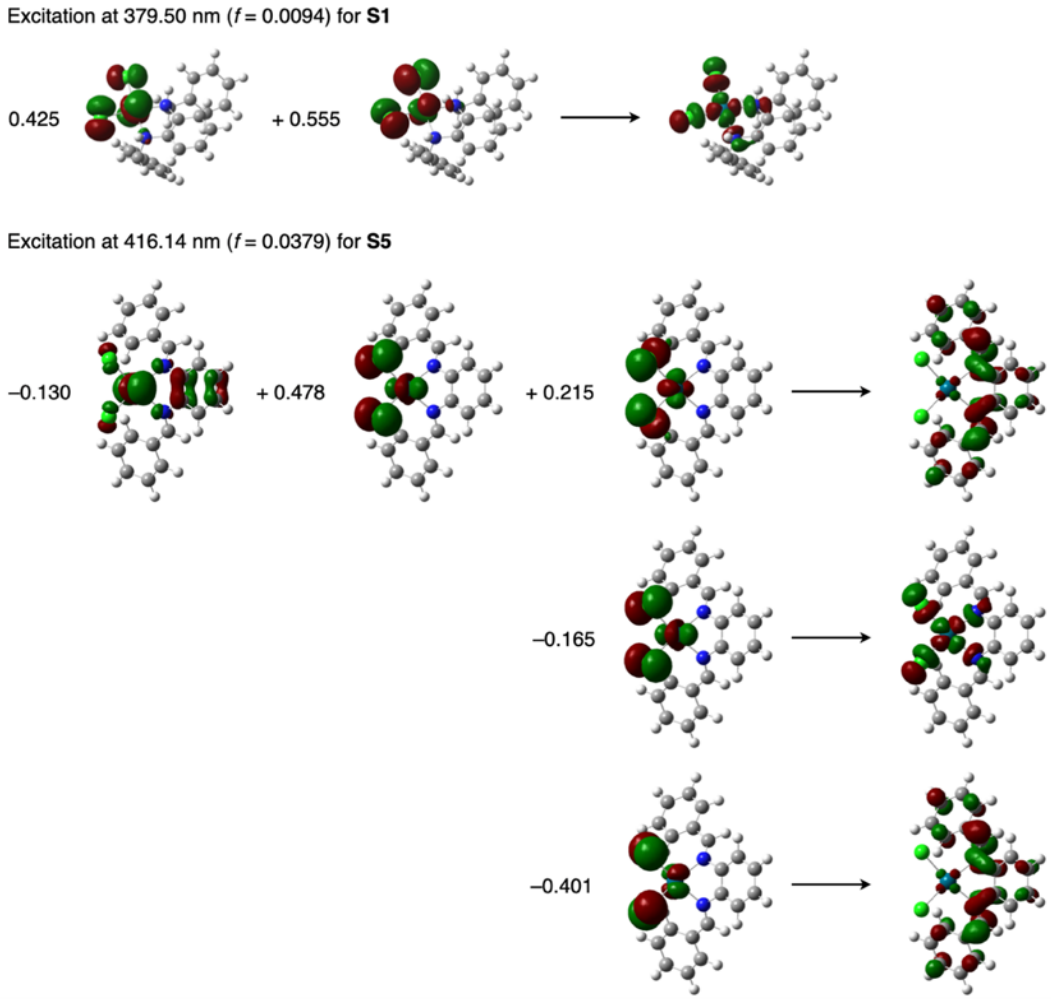

Fig. S20 Assignment of the excitations for S1 and S5.

Reduction of $HAuCl_4$ with millimeter-scale MMF single crystals

Experimental procedure: To a mixed solution of $HAuCl_4 \cdot 4H_2O$ (0.40 mM, 0.84 μmol) and L-Asc (40 mM, 84 μmol, 100 eq) in CH_3CN–CH_3OH (2.1 mL, 4:1 v/v), millimeter-scale crystals of MMF (0.79 mg, 0.68 μmol, 0.81 eq) were added and stirred at room temperature for 30 min. The resulting solid components were collected by filtration, washed with CH_3OH and dried in air.

The solid-state UV-vis absorption spectrum and the PXRD patterns of the product did not show the formation of AuNPs (Figs. S21 and S22).

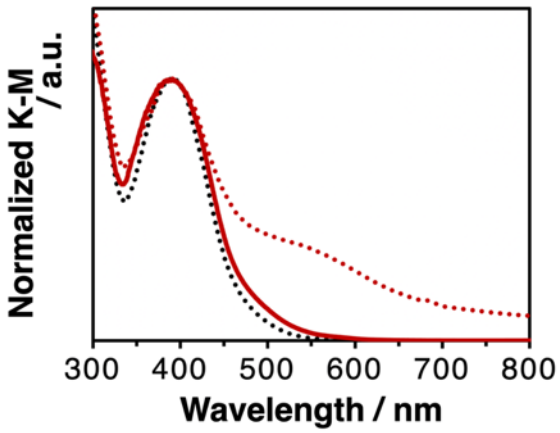

Fig. S21 Solid-state absorption (Kubelka-Munk function, rt) spectra of millimeter-scale MMF crystals. Millimeter-scaled MMF crystals before (black dotted line) and after (red solid line) the reaction with $HAuCl_4 \cdot 4H_2O$ with L-Asc. The red dotted line shows a spectrum of typical AuNK/MMF.

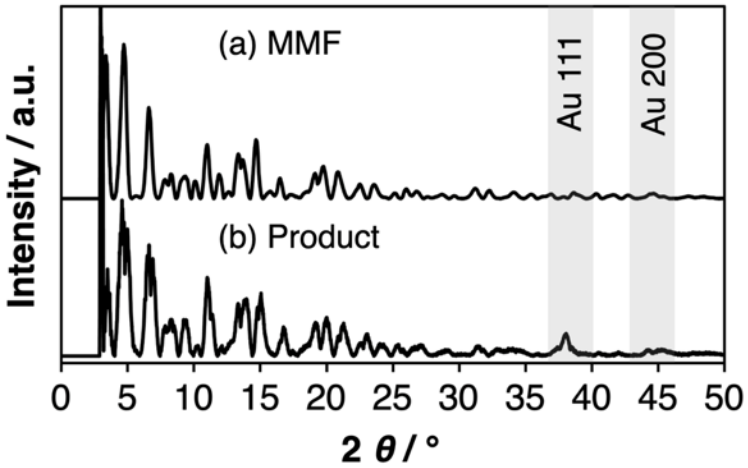

Fig. S22 Powder X-ray diffraction patterns (20 °C) of MMF. (a) As-synthesized MMF. (b) Millimeter-scale MMF after the reaction with $HAuCl_4 \cdot 4H_2O$ with L-Asc.

Reduction of $HAuCl_4$ with Pd_2LCl_4 crystals

Preparation of Pd_2LCl_4 single crystals: A solution of **L** (5.18 mg, 8.21 μmol, 29.0 mL, 0.283 mM) in CH_3CN was heated up to 80 °C. To this solution added a solution of $PdCl_2(CH_3CN)_2$ (2.25 mg, 8.67 μmol, 0.434 mL, 20.0 mM, 1.06 eq) in CH_3CN. The yellow solution was filtered and allowed to stand for 5 d at room temperature to afford yellow crystals suitable for XRD analysis.

When ligand **L** was reacted with half the usual amount of $PdCl_2(CH_3CN)_2$, a dinuclear complex

Pd_2**L**Cl_4 with a different crystal system was obtained (Fig. S23).

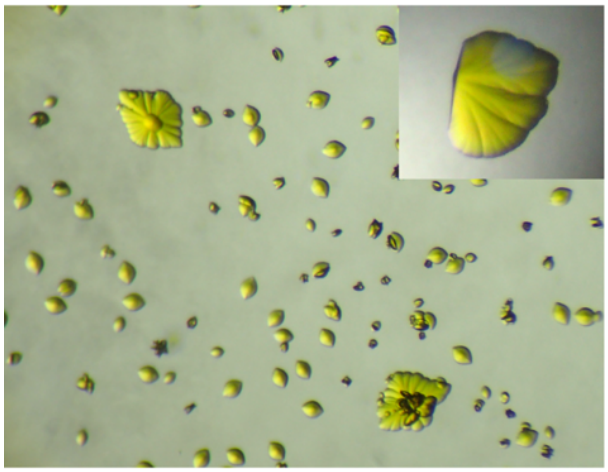

Fig. S23 Photograph of the obtained Pd_2**L**Cl_4 crystals. The inset shows a single crystal subjected to the XRD analysis.

Crystal data for $Pd_2LCl_4\cdot(CH_3CN)\cdot(H_2O)_{0.5}$: $C_{44}H_{45}Cl_4N_7O_{0.5}Pd_2$, Fw = 1034.47, crystal dimensions 0.17 × 0.13 × 0.08 mm^3, orthorhombic, space group *Pnma*, a = 13.2066(2), b = 23.2676(4), c = 14.0442(3) Å, V = 4315.58(14) Å, Z = 4, ρ_{calcd} = 1.592 g cm^{-3}, μ = 9.334 mm^{-1}, T = 93 K, λ(CuKα) = 1.54184 Å, $2\theta_{max}$ = 146.814°, 13527/4336 reflections collected/unique (R_{int} = 0.0358), R_1 = 0.0685 ($I > 2\sigma(I)$), wR_2 = 0.2127 (for all data), GOF = 1.077, largest diff. peak and hole 2.21/–1.31 e Å^{-3}. Hydrogen atoms of the water molecule were not assigned because the orientation of the molecule cannot be determined. CCDC deposition number 2093923.

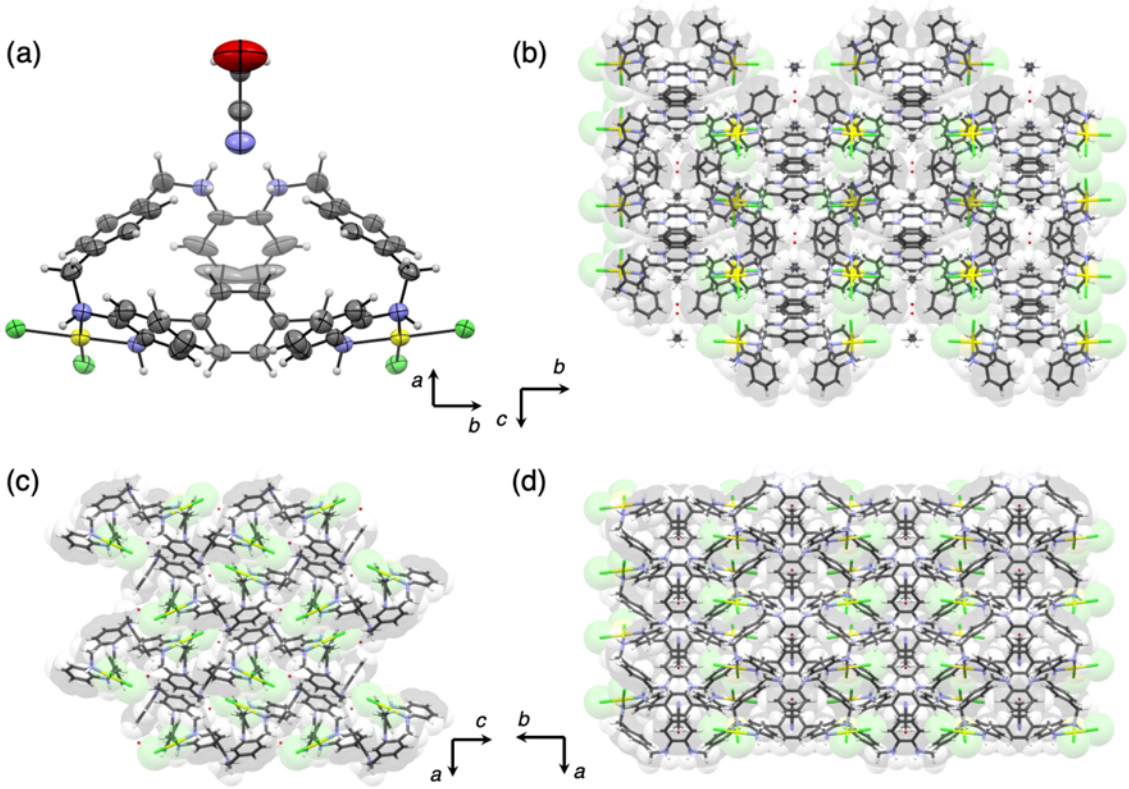

Fig. S24 Crystal structure of Pd_2**L**$Cl_4 \cdot (CH_3CN) \cdot (H_2O)_{0.5}$. (a) ORTEP diagram (50% probability). Packing structure from (b) *a*, (c) *b* and (d) *c* axes. Color code: gray C, white H, lime Cl, blue N, red O, yellow Pd.

Preparation of Pd_2L**Cl_4 microcrystals:** A solution of **L** (15.7 mg, 24.9 μmol, 88.0 mL, 0.283 mM) in CH_3CN was heated up to 80 °C. To this solution added a solution of $PdCl_2(CH_3CN)_2$ (6.99 mg, 26.9 μmol, 1.34 mL, 20.1 mM, 1.08 eq) in CH_3CN and stirred at room temperature for 17.5 h. The solid components were collected, washed well with CH_3CN and dried in vacuum to yield Pd_2**L**$Cl_4 \cdot (CH_3CN)_{0.64} \cdot (H_2O)_{0.90}$ (10.3 mg, 9.98 μmol, 80%).

Elemental analysis: calcd for $C_{42}H_{42}Cl_4N_6Pd_2 \cdot (CH_3CN)_{0.64} \cdot (H_2O)_{0.90}$: C 50.56%, H 4.49%, N 9.05%; found C 50.59%, H 4.53%, N 8.92%.

The ^{1}H NMR spectrum of a solution of vacuum-dried Pd_2**L**Cl_4 in DMSO-d_6 contains a set of signals of Pd-free ligand **L** and Pd_3**L**Cl_6, indicating that Pd_2**L**Cl_4 undergoes self-metal exchange in solution. DCl-DMSO-d_6 (0.1 M) was used to dissociate the coordination bonds of Pd_3**L**Cl_6 and the molar ratio of ligand **L** to CH_3CN was estimated, and the number of included solvent molecules contained was calculated from the number of methylene protons of **L** (Fig. S25). The calculated molar ratio, **L**/CH_3CN = 1:0.64, was consistent with the result of elemental analysis.

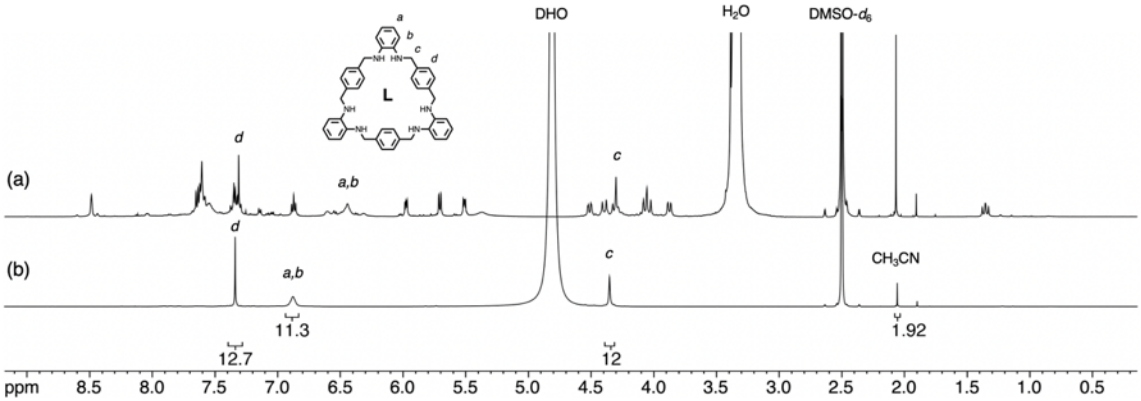

Fig. S25 ^{1}H NMR spectra (500 MHz, 300 K) of the components of Pd_2**L**Cl_4. (a) Pd_2**L**Cl_4 in DMSO-d_6. (b) Pd_2**L**Cl_4 in DCl-DMSO-d_6 (0.1 M).

The PXRD pattern of Pd_2**L**Cl_4 microcrystals was in a good agreement with the calculated pattern (Fig. S26).

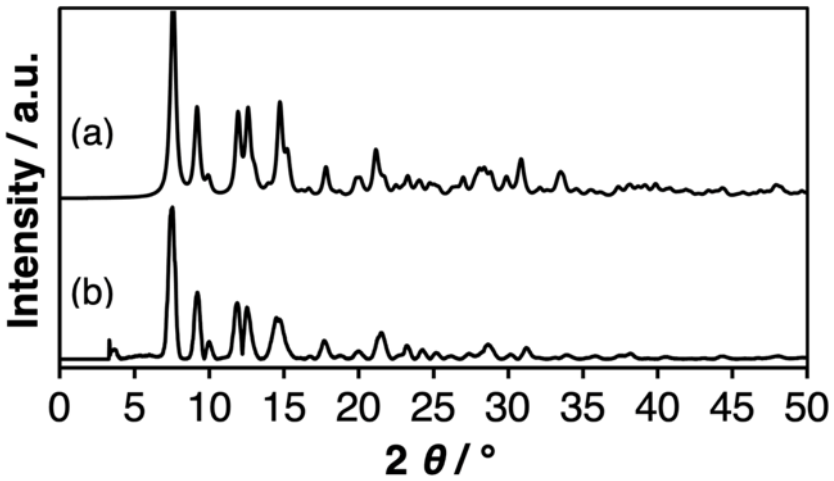

Fig. S26 Powder X-ray diffraction patterns (20 °C) of Pd_2**L**Cl_4. (a) Pd_2**L**Cl_4 simulated from the single-crystal structure. (b) As-synthesized Pd_2**L**Cl_4 microcrystals.

The microscopic shape of the product was similar to that of rounded Pd_2**L**Cl_4 single crystals (Fig. S27). Some rhombic crystals of Pd_3**L**Cl_6 (MMF) were included in the sample.

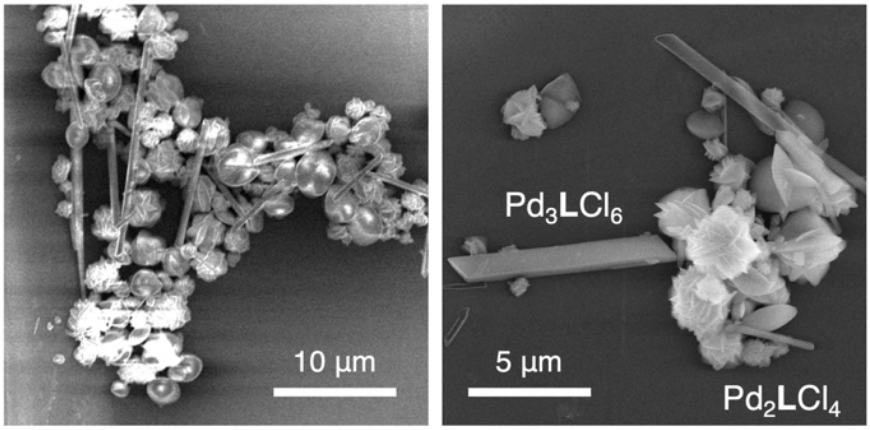

Fig. S27 Representative SEM images of Pd_2**L**Cl_4 microcrystals including Pd_3**L**Cl_6 (MMF). Measurement conditions: 2.00 kV, 6.3 pA for the left image; 10.00 kV, 6.3 pA for the right image.

AuNK synthesis with Pd_2L**Cl_4 microcrystals:** To a mixed solution of $HAuCl_4 \cdot 4H_2O$ (0.40 mM, 0.69 µmol) and L-Asc (40 mM, 69 µmol, 100 eq) in CH_3CN–CH_3OH (1.7 mL, 4:1 v/v), Pd_2**L**Cl_4 microcrystals (0.54 mg, 0.55 µmol, 0.80 eq) were added and stirred at room temperature for 30 min. The solid components were collected, washed with CH_3OH and dried in air.

A large broad shoulder around 550 nm was observed around 550 nm in the solid-state absorption spectrum of the product, suggesting the formation of AuNPs (Fig. S28). The PXRD pattern of the Pd_2**L**Cl_4 microcrystals after the reaction showed diffraction peaks of 111 and 200 for Au (Fig. S29). As a result of SEM observation, we found that AuNKs were formed on the surface of Pd_2**L**Cl_4 microcrystals (Fig. S30).

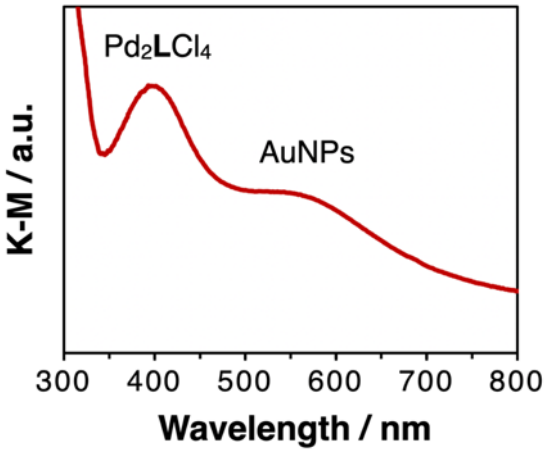

Fig. S28 Solid-state absorption (Kubelka-Munk function) spectrum of Pd_2**L**Cl_4 microcrystals

after the reaction with $HAuCl_4 \cdot 4H_2O$ and L-Asc.

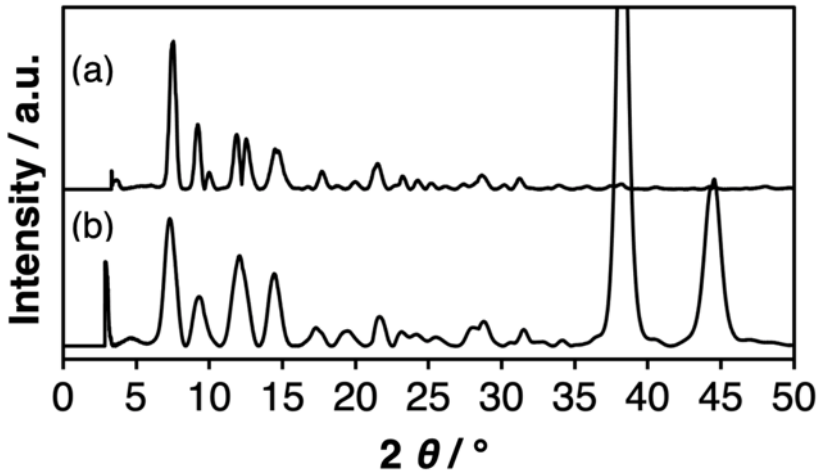

Fig. S29 Powder X-ray diffraction patterns (20 °C) of Pd_2**L**Cl_4 microcrystals. Pd_2**L**Cl_4 microcrystals (a) before and (b) after the reaction with $HAuCl_4 \cdot 4H_2O$ with L-Asc.

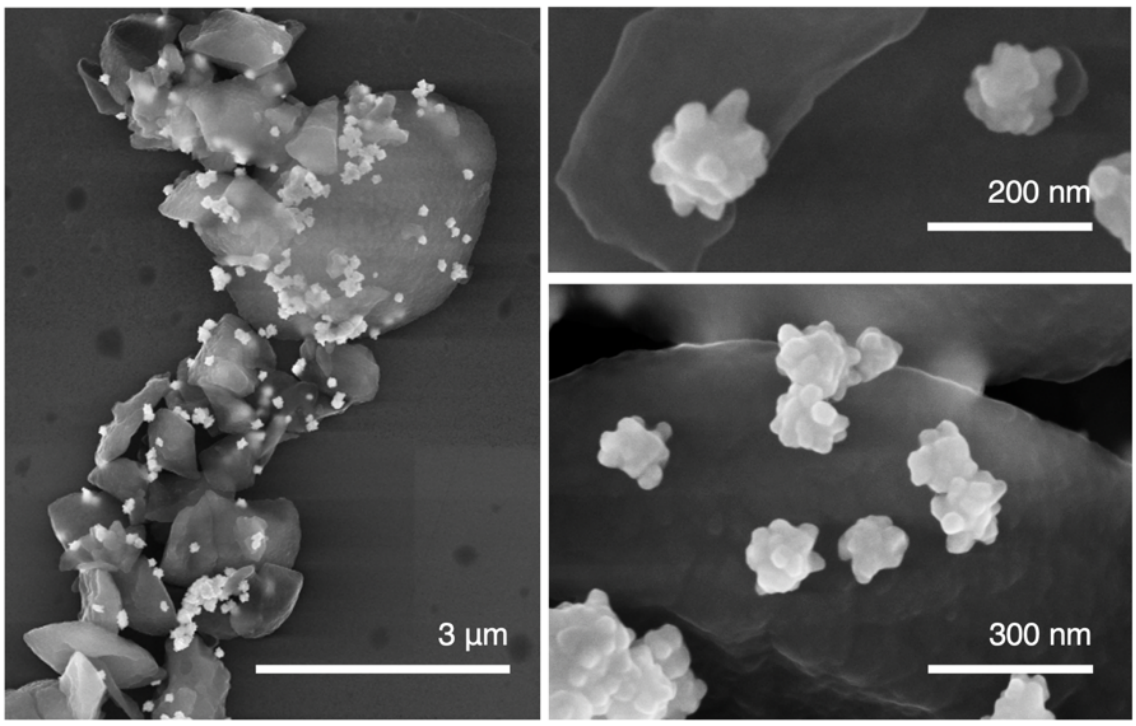

Fig. S30 Representative SEM images (15.00 kV, 0.20 nA) of Pd_2**L**Cl_4 microcrystals depositing AuNKs.

S4. Growth of AuNKs over time on MMF crystals

Time-course observation of AuNKs with SEM

Experimental procedure: As a typical method, MMF microcrystals (0.5 mg, 0.80 eq) were dispersed in a solution of $HAuCl_4 \cdot 4H_2O$ (0.50 mM) in CH_3CN and mixed with a solution of L-Asc (0.20 M, 100 eq) in CH_3OH. The suspension was stirred for 0.5–30 min at room temperature. The solid components were collected, washed with CH_3OH and dried in air.

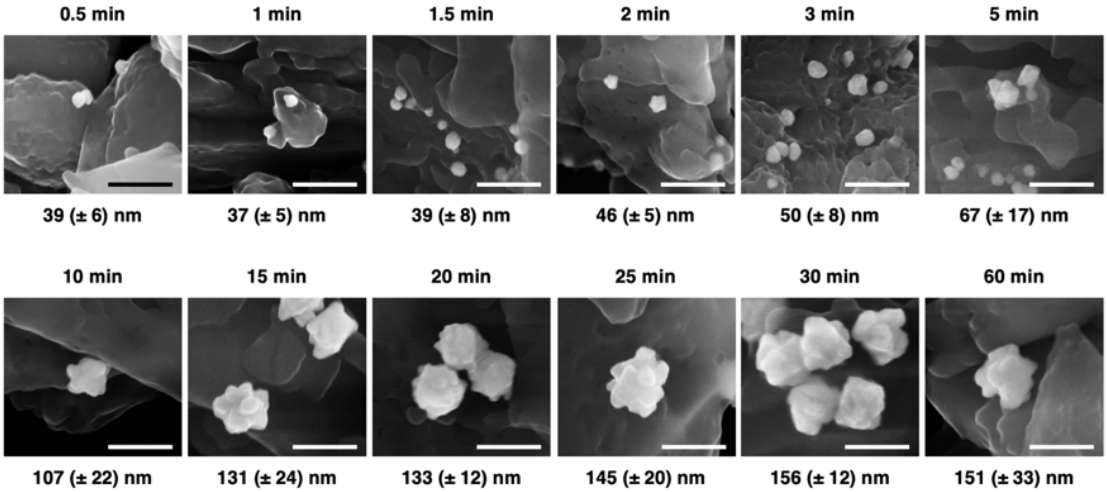

Fig. S31 SEM images (15.00 kV, 0.20 nA) of AuNP/MMF obtained by the time-course reactions. Scale bars: 200 nm.

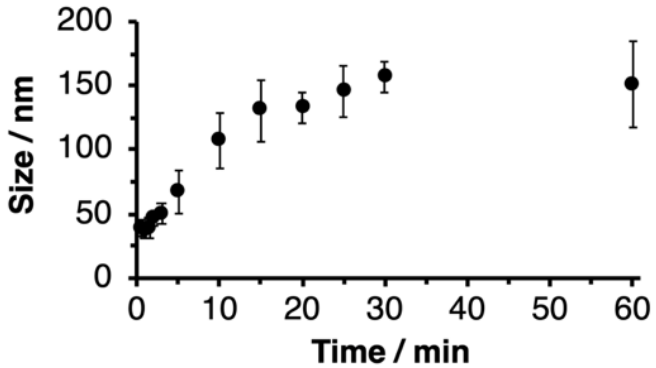

Fig. S32 Plot of the AuNP size distribution as a function of reaction time.

Zeta potential measurement

			Mean (mV)	Area (%)	St Dev (mV)
Zeta Potential (mV):	-12.2	**Peak 1:**	-12.2	100.0	4.72
Zeta Deviation (mV):	4.72	**Peak 2:**	0.00	0.0	0.00
Conductivity (mS/cm):	0.0215	**Peak 3:**	0.00	0.0	0.00
Result quality	Good				

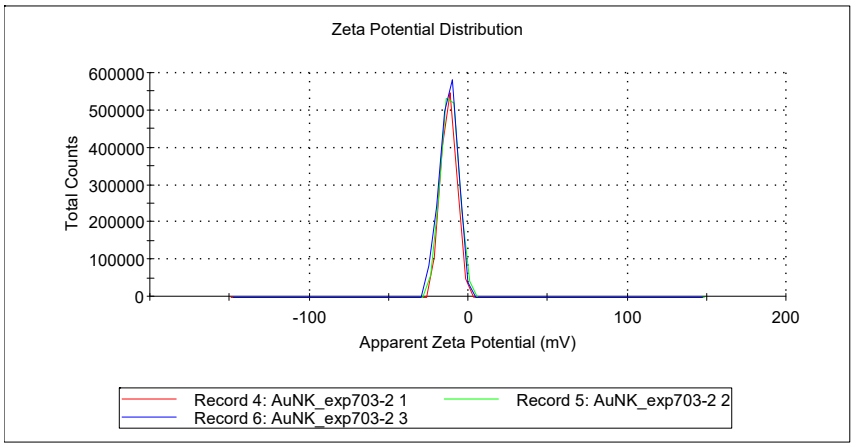

Fig. S33 Zeta potential distribution of AuNKs suspended in CH_3OH.

			Mean (mV)	Area (%)	St Dev (mV)
Zeta Potential (mV):	43.3	**Peak 1:**	43.3	100.0	9.79
Zeta Deviation (mV):	9.79	**Peak 2:**	0.00	0.0	0.00
Conductivity (mS/cm):	0.00751	**Peak 3:**	0.00	0.0	0.00
Result quality	Good				

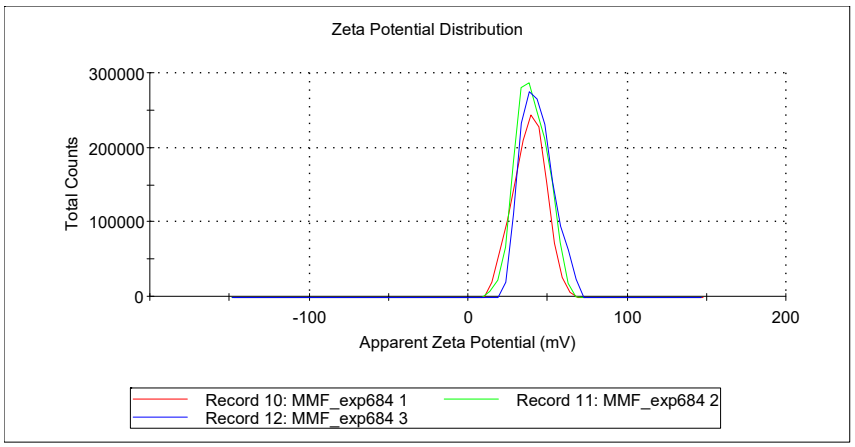

Fig. S34 Zeta potential distribution of MMF microcrystals dispersed in CH_3OH.

Two-step growth of AuNKs on MMF

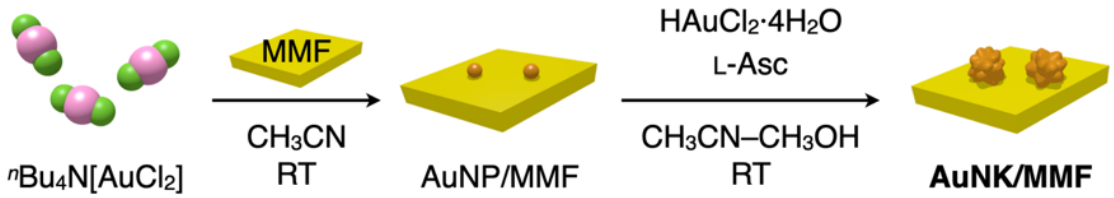

First step: MMF microcrystals (1.25 mg, 1.07 μmol, 0.80 eq) were dispersed into a solution of $^{n}Bu_4N[AuCl_2]$ (1.00 mM, 1.34 mL, 1.34 μmol) in CH_3CN and stirred at room temperature for 30 min. The brown solid components were collected, washed with CH_3CN and dried in air (AuNP/MMF, 1.09 mg).

Second step: To a solution of L-Asc (0.20 M, 0.26 mL, 52 μmol, 100 eq), AuNP/MMF (0.49 mg) in CH_3OH dispersed in a solution of $HAuCl_4·4H_2O$ (0.50 mM, 1.05 mL, 0.52 μmol) in CH_3CN was added and stirred at room temperature for 30 min. The brown solid components were collected washed with CH_3OH and dried in air (AuNK/MMF).

In the solid-state UV-vis absorption spectra (Fig. S35), a broad absorption band around 530 nm was observed after the first reaction with $^{n}Bu_4N[AuCl_2]$, and a larger and broader absorption band appeared during the second reaction with $HAuCl_4·4H_2O$ and L-Asc. This spectral change suggests a stepwise growth of AuNPs on MMF crystals, which was also supported by SEM observation (Fig. S36). The small irregularly shaped AuNPs formed in the first reaction grew into monodispersed AuNKs in the second reaction. This two-step growth of AuNKs suggests that the initially formed small AuNPs serve as seed particles for further growth on the crystal surface of MMF.

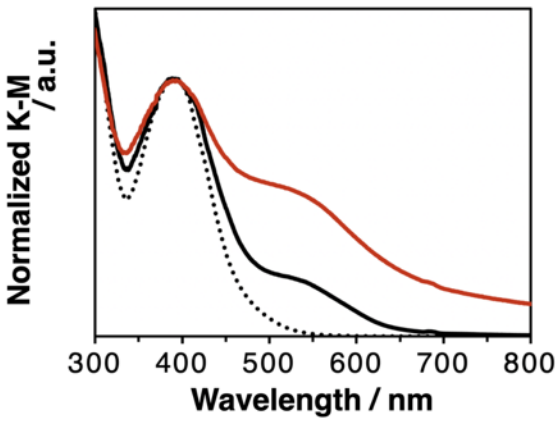

Fig. S35 Solid-state absorption (Kubelka-Munk function) spectra of MMF microcrystals. MMF before the reactions (black dotted line), after the first reaction with $^{n}Bu_4N[AuCl_2]$ (black solid line) and after the second reaction with $HAuCl_4·4H_2O$ and L-Asc (red solid line).

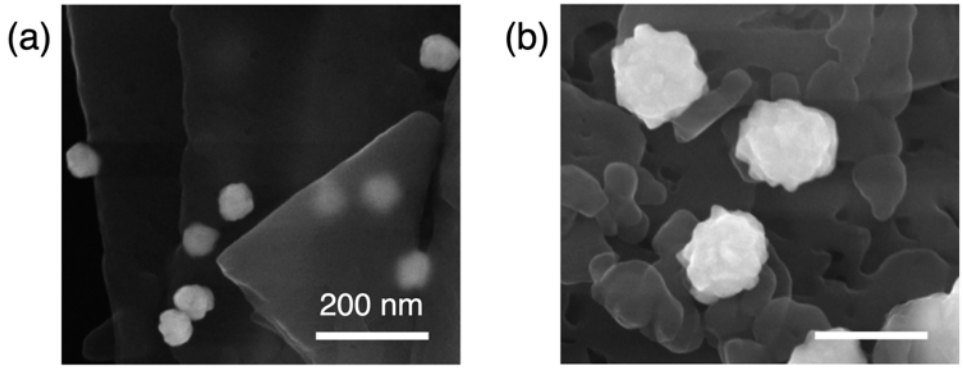

Fig. S36 Representative SEM images (15.00 kV, 0.20 nA) of MMF microcrystals. MMF (a) after the first reaction with $^{n}Bu_4N[AuCl_2]$ and (b) after the second reaction with $HAuCl_4 \cdot 4H_2O$ and L-Asc.

***In-situ* observation of the AuNP growth with HS-AFM**

Experimental procedure: MMF microcrystals were fixed on a cylindrical glass stage with a diameter of 2 mm and a height of 3 mm using a thin paste of wax (Red Sticky Wax SS-66, Universal Photonics). The whole glass stage containing the MMF crystals was immersed in a mixed solution of $HAuCl_4 \cdot 4H_2O$ (0.40 mM) and L-Asc (40 mM) in CH_3CN–CH_3OH (4:1 v/v, solution A) for 5 min to form AuNPs on the surface of the MMF crystals. Then, they were dried overnight under vacuum in an aspirator to firmly fix the AuNPs to the crystal surface. To observe the growth of AuNPs *in-situ*, the above sample with pre-grown AuNPs was immersed in CH_3CN and searched for AuNPs by HS-AFM imaging. Once AuNPs were found, the observation solution was quickly changed from CH_3CN to the solution A, and the re-growth of the AuNPs was observed for 5 to 20 min (Figs. S37–S39 and Supporting Movies 1–3).

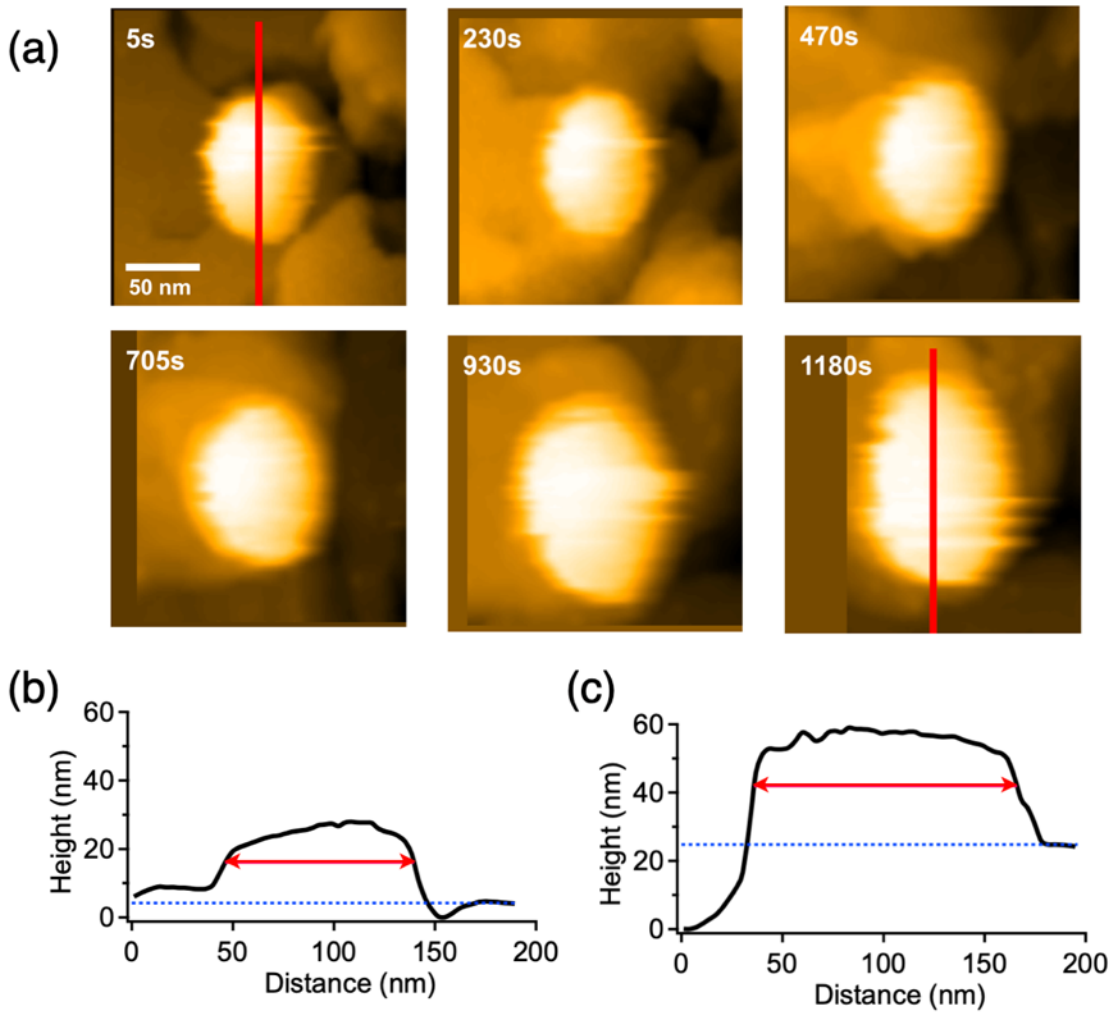

Fig. S37 *In-situ* observation of the growth of a 100-nm AuNP on MMF surface by HS-AFM. (a) Clipped AFM images showing the AuNP growing on microcrystalline surface of MMF with the imaging rate of 5 s/frame. The height profiles of the AuNP corresponding to the red lines after (b) 5 s and (c) 1180 s of growth. Red bidirectional arrows correspond to the widths at the half maxima from the baselines indicated by the dotted lines. The widths of the AuNP before and after the growth were ~90 nm and ~130 nm, respectively.

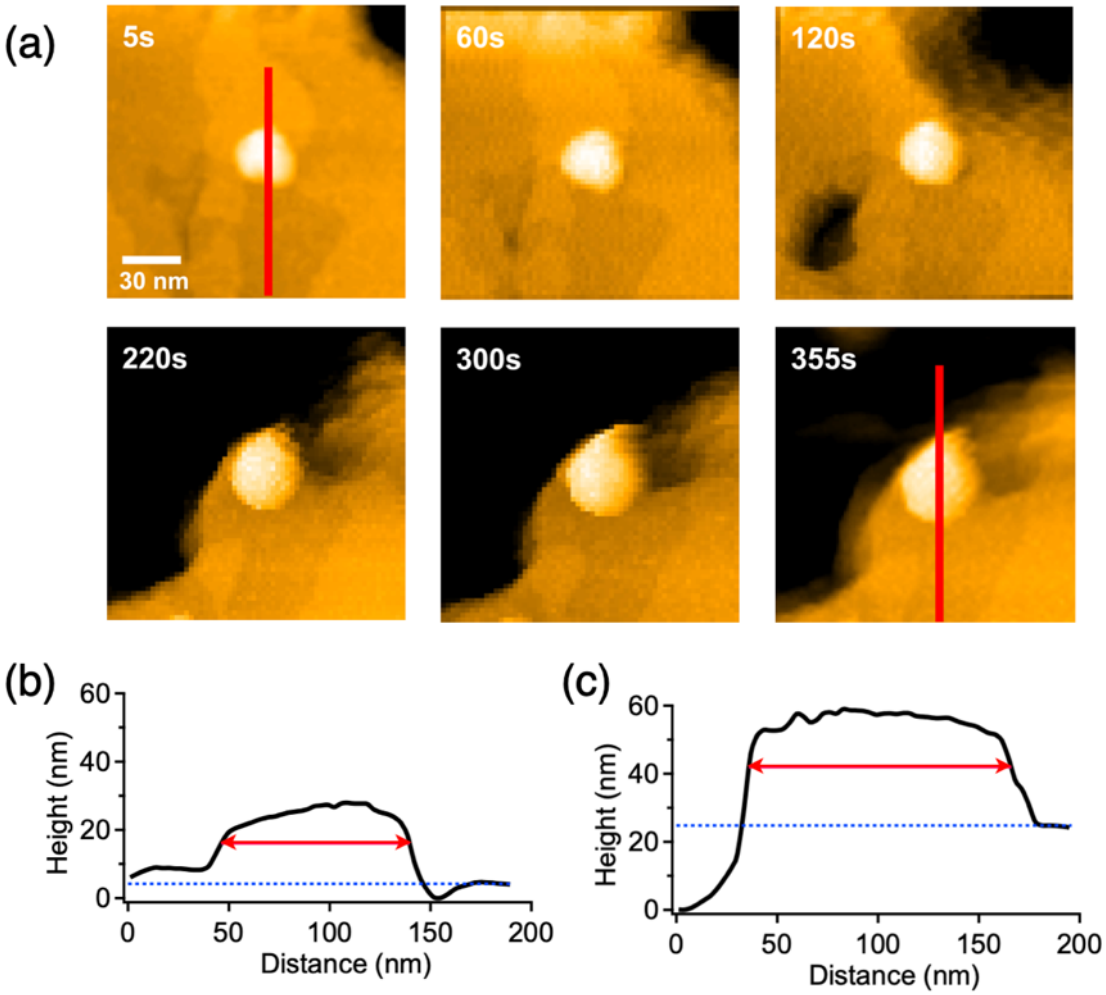

Fig. S38 *In-situ* observation of the growth of a 30-nm AuNP on MMF surface by HS-AFM. (a) Clipped AFM images showing the AuNP growing on microcrystalline surface of MMF with the imaging rate of 5 s/frame. The height profiles of the AuNP corresponding to the red lines after (b) 5 s and (c) 355 s of growth. Red bidirectional arrows correspond to the widths at the half maxima from the baselines indicated by the dotted lines. The widths of the AuNP before and after the growth were ~26 nm and ~40 nm, respectively.

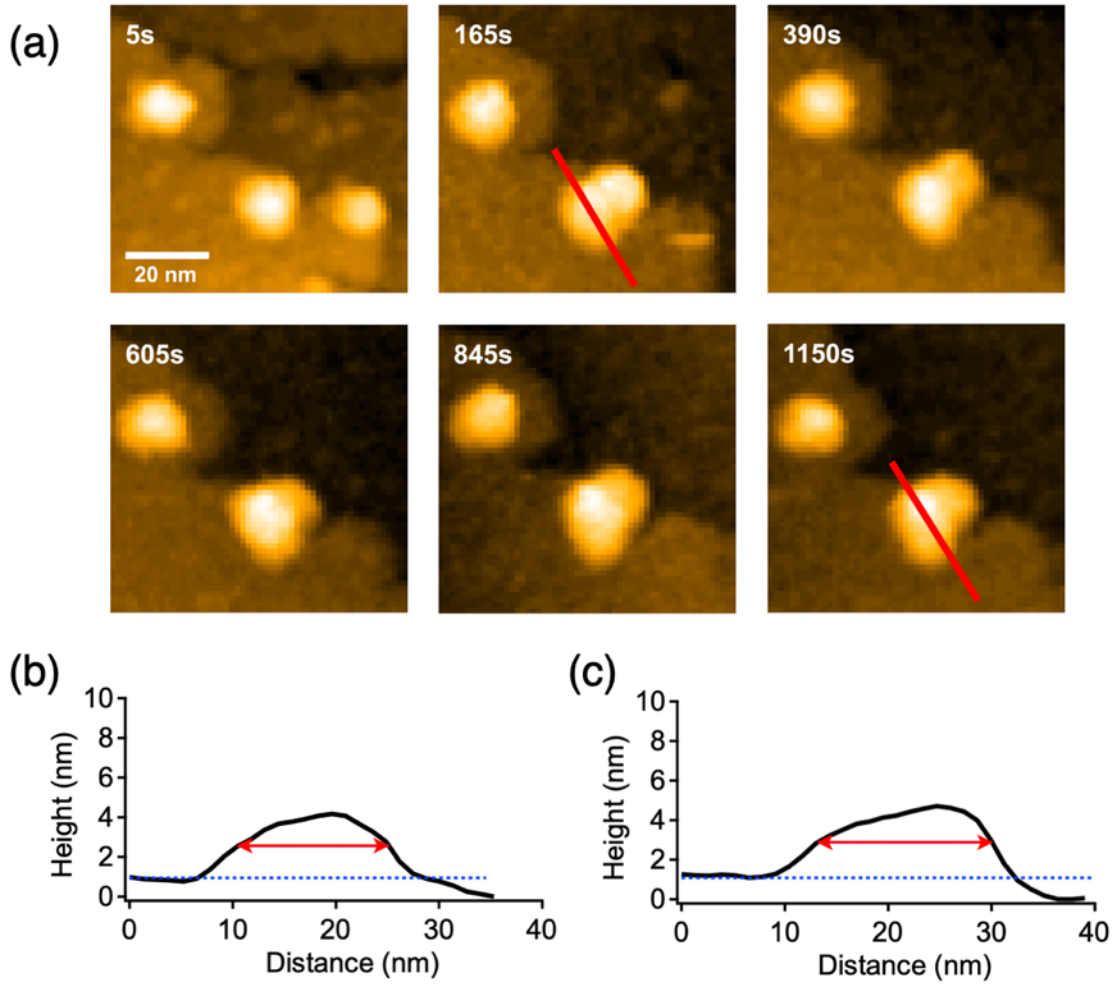

Fig. S39 Fusion and growth of AuNPs. (a) Clipped AFM images showing the fusion and subsequent growth of two small AuNPs on MMF surface. Height profiles of the fused AuNP corresponding to the red lines after (b) 165 s and (c) 1150 s of growth. The red bidirectional arrows correspond to the widths at the half maxima from the baselines indicated by the dotted lines. The widths of the AuNP before and after the growth were ~14 nm and ~17 nm, respectively.

Time-course observation of AuNKs with TEM

Experimental procedure: Microcrystals of MMF reacted with $HAuCl_4 \cdot 4H_2O$ and L-Asc at room temperature for (i) 0.5 and (ii) 30 min were suspended in DMSO to dissolve the MMF moiety. For (i), the black precipitate obtained was collected by centrifugation twice in DMSO and washed twice with CH_3OH. It was resuspended in CH_3OH, cast on a micro grid and dried in air. For (ii), the DMSO

suspension of the black precipitate was cast directly onto a micro grid, washed with drops of DMSO and CH_3OH and dried in air.

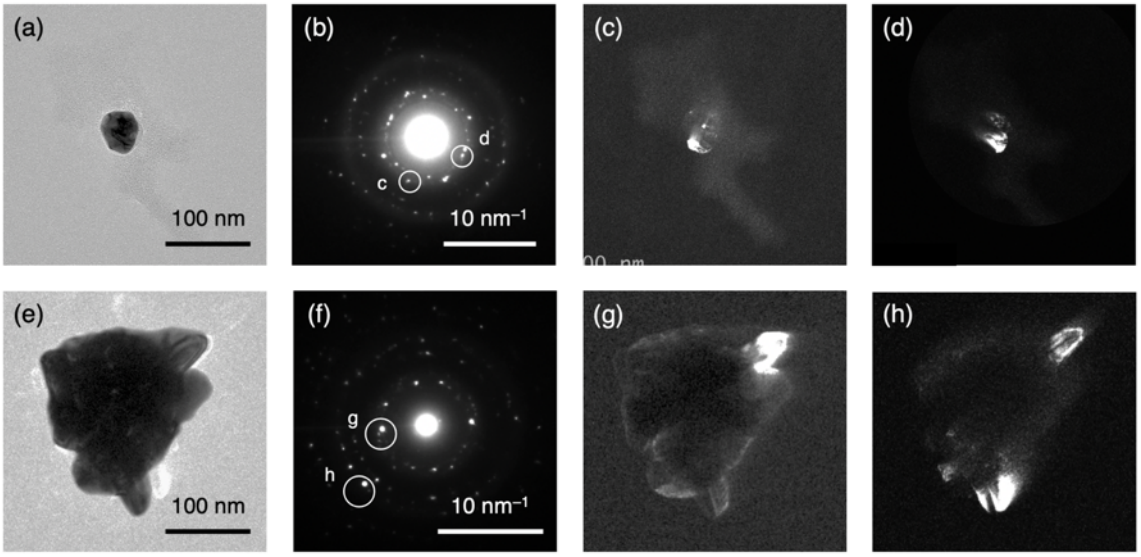

Fig. S40 TEM analysis of AuNPs isolated from MMF. (a,e) Representative TEM images (200 kV), (b,f) ED patterns, and (c,d and g,h)dark-field images corresponding to the selected diffractions (marked by white circles in ED) of AuNPs obtained by the reactions for (a–d) 0.5 min and (e–h) 30 min, respectively.

S5. Demonstration of SERS effects of AuNKs

As a proof-of-concept experiment, AuNKs isolated from MMF microcrystals were investigated as a Raman sensor using the surface-enhanced Raman scattering (SERS) effect. For comparison, previously-reported branched AuNPs (star-like gold nanoparticles, SGNs)[12] synthesized by a one-step reduction of $HAuCl_4 \cdot 4H_2O$ using hydroquinone and sodium citrate were also used as a SERS effector. Congo red (CR), one of the most famous azo dyes, was used as an analyte.

Characterizations

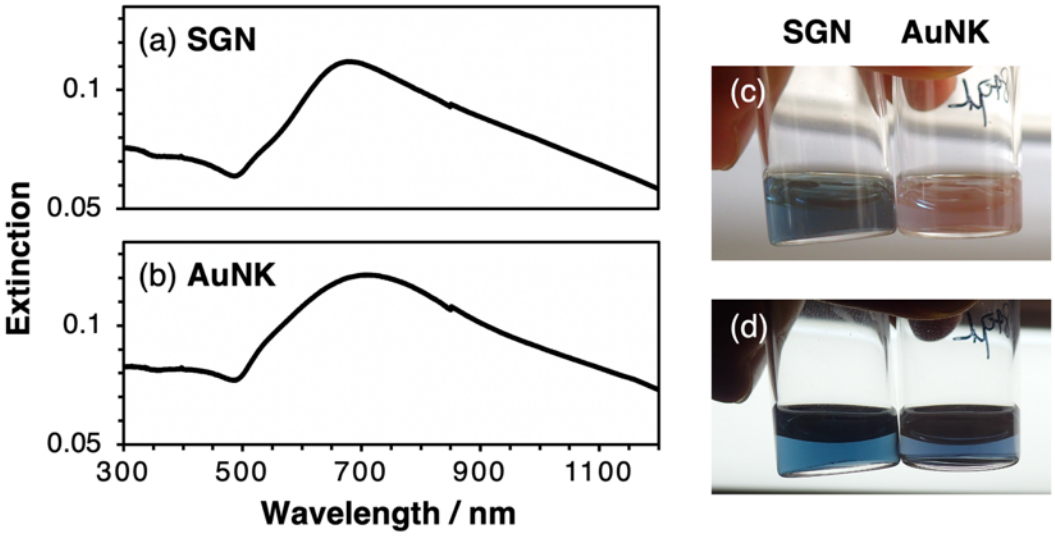

Fig. S41 Extinction spectra (20 °C) of the branched AuNPs suspended in water. (a) SGNs. (b) AuNKs. Photographs of the aqueous suspensions of SGNs (left) and AuNKs (right) taken in (c) ambient light and (d) transmitted light.

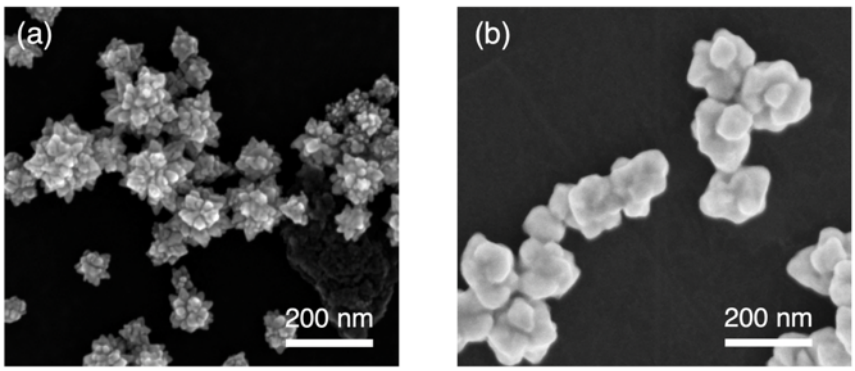

Fig. S42 Representative SEM images of AuNPs used for SERS demonstration. (a) SGNs (15.00 kV, 0.20 nA). (b) AuNKs (5.00 kV, 50 pA).

SERS measurement

Experimental procedure: In a micro tube, 100 µL of an aqueous CR solution (10 µM, 1.0 nmol, 0.70 µg) was mixed with an equal volume of an aqueous AuNK or SGN suspension containing approximately 0.01 mg of the particles, of which 30 µL was caste onto a silicon wafer substrate. After the microscope was focused on the sample, Raman spectra were recorded with an exposure time 5 seconds at room temperature and a cumulative total of 10 scans. For each sample, the three spectra obtained at different points were averaged (Fig. S43). For the spectra shown in Fig. S44, a manual baseline correction was performed before averaging.

No characteristic signals were found in the aqueous solution of CR at a concentration of 5 µM (Fig. S44c). In AuNKs or SGNs, some signals were slightly enhanced (Fig. S44a,b). The signal enhancement was comparable for both AuNKs and SGNs, suggesting that AuNKs as well as SGNs are promising SERS sensors.

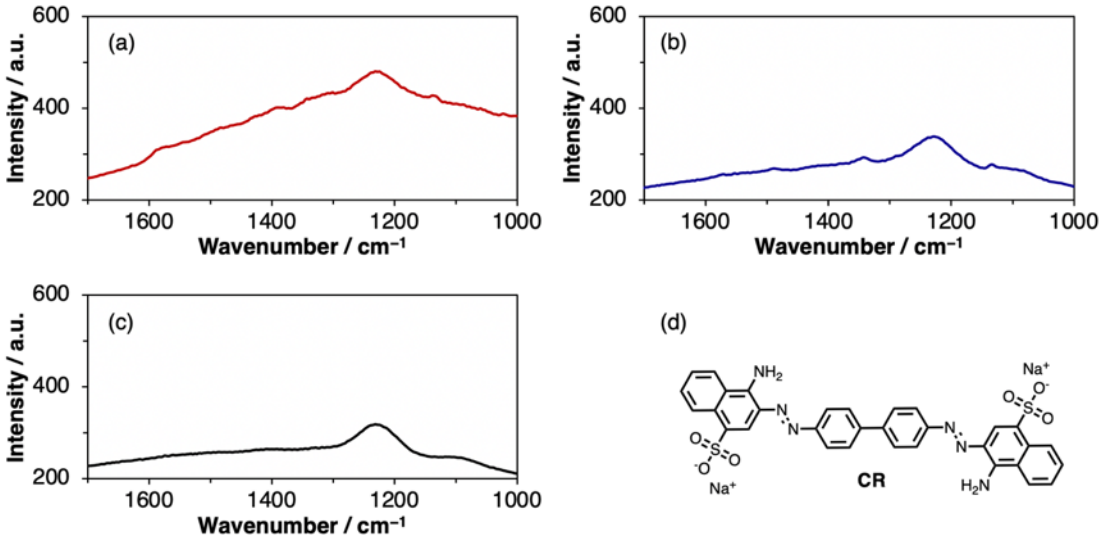

Fig. S43 Raman spectra of CR. (a) With AuNKs. (b) With SGNs. (c) Without AuNPs. (d) Chemical structure of CR.

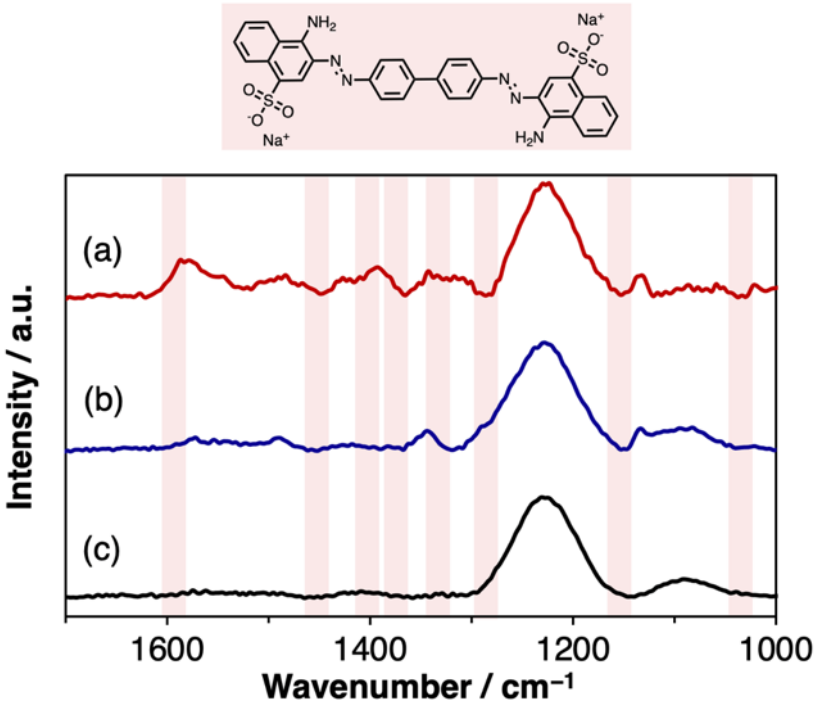

Fig. S44 Baseline-corrected Raman spectra of CR. (a) With AuNKs. (b) With SGNs. (c) Without AuNPs. The pink bands show the wavenumber region where the Raman signals of CR should appear.

S6. References

1 S. Tashiro, R. Kubota and M. Shionoya, *J. Am. Chem. Soc.*, 2012, **134**, 2461–2464.

2 R. W. Buckley, P. C. Healy and W. A. Loughlin, *Aust. J. Chem.*, 1997, **50**, 775–778.

3 O. V. Dolomanov, L. J. Bourhis, R. J. Gildea, J. a. K. Howard and H. Puschmann, *J. Appl. Crystallogr.*, 2009, **42**, 339–341.

4 G. M. Sheldrick, *Acta Crystallogr. A*, 2008, **64**, 112–122.

5 T. Ando, T. Uchihashi and T. Fukuma, *Prog. Surf. Sci.*, 2008, **83**, 337–437.

6 D. Herebian, E. Bothe, F. Neese, T. Weyhermüller and K. Wieghardt, *J. Am. Chem. Soc.*, 2003, **125**, 9116–9128.

7 U. Koelle and A. Laguna, *Inorg. Chim. Acta*, 1999, **290**, 44–50.

8 L. Aldous, D. S. Silvester, C. Villagrán, W. R. Pitner, R. G. Compton, M. Cristina Lagunas and C. Hardacre, *New J. Chem.*, 2006, **30**, 1576–1583.

9 B. Ballarin, L. Busetto, M. Cristina Cassani, C. Femoni, *Inorg. Chim. Acta*, 2010, **363**, 2055–2064.

10 A. D. Becke, *J. Chem. Phys.*, 1993, **98**, 5648–5652.

11 P. J. Hay and W. R. Wadt, *J. Chem. Phys.*, 1985, **82**, 299–310.

12 C. Morasso, D. Mehn, R. Vanna, M. Bedoni, E. Forvi, M. Colombo, D. Prosperi and F. Gramatica, *Mater. Chem. Phys.*, 2014, **143**, 1215–1221.

Cartesian coordinated of calculated structures of model complexes S1 to S5

S1

Pd	-1.57490156	-1.09222717	-0.22705365
Cl	-1.14835357	-3.21074947	0.66433942
Cl	-3.90673988	-1.17247110	-0.05458116
N	0.49469597	-0.81967490	-0.52877080
H	0.80826534	-1.72346575	-0.88910232
N	-1.70860090	0.80534837	-1.15204715
H	-2.43487158	0.62830525	-1.85057774
C	-0.43829120	1.04198147	-1.83814850
C	2.72228797	-0.71916490	0.69854720
C	3.29338517	-1.99842672	0.59626857
H	2.64914328	-2.87625732	0.59223822
C	0.65399929	0.21046464	-1.55113123
C	-1.40315275	2.19473608	0.94706384
C	1.21909767	-0.56869281	0.77825860
H	0.79714691	-1.29999597	1.47156077
H	0.93359207	0.43011621	1.11094656
C	-2.21989044	1.94118253	-0.29717604
H	-2.26427148	2.84789869	-0.91371706
H	-3.23909994	1.64695132	-0.03555454
C	4.67936589	-2.15447065	0.52123419
H	5.10756184	-3.15067212	0.44636865
C	-0.32471187	2.02911099	-2.82136600
H	-1.18012601	2.65873182	-3.05320531
C	1.84501502	0.35900334	-2.27125247
H	2.68145429	-0.30039941	-2.06553561
C	1.95152833	1.34258545	-3.25654225
H	2.87740165	1.44441554	-3.81539699
C	3.56797875	0.39776453	0.74545765
H	3.13691870	1.39193153	0.83965529
C	0.86880317	2.18265323	-3.52902747
H	0.94413127	2.94158395	-4.30257630
C	5.51437296	-1.03208642	0.55986069
H	6.59331367	-1.15325759	

		0.50867445	
C	-0.39477332	3.16954175	0.96040092
H	-0.19199202	3.74778597	0.06142560
C	-1.67056737	1.47524928	2.12294793
H	-2.45601659	0.72366601	2.12396952
C	4.95627553	0.24395611	0.67809627
H	5.60003766	1.11896068	0.72030153
C	-0.93130625	1.71720106	3.28323686
H	-1.14918427	1.15359672	4.18648026
C	0.34640954	3.41252813	2.12152590
H	1.12101343	4.17536385	2.11941003
C	0.07989028	2.68441226	3.28488058
H	0.65067837	2.87504930	4.19012656
S2			
Pd	0.00002729	-1.39434248	-0.00001373
Cl	1.56247715	-3.12970705	0.78381644
Cl	-1.56229397	-3.12980644	-0.78373473
N	1.22531843	0.17708381	0.47520448
N	-1.22532650	0.17701193	-0.47528087
C	-0.66096112	1.41580395	-

		0.29437595	
C	3.72775993	0.42256438	0.42969634
C	3.76425542	0.35023476	-0.97011378
H	2.84543643	0.08662594	-1.48676357
C	0.66085554	1.41584862	0.29434566
C	-3.72776481	0.42245930	-0.42972673
C	2.45629276	0.07420256	1.20837944
H	2.55753263	-0.96882014	1.53236031
H	2.44093971	0.69775161	2.12735285
C	-2.45630606	0.07408446	-1.2084235
H	-2.44098265	0.69761285	-2.12741602
H	-2.55754064	-0.96895222	-1.53236825
C	4.94505434	0.61204740	-1.67009106
H	4.94956695	0.55173895	-2.75772056
C	-1.26366319	2.65224236	-0.60417349
H	-2.25966490	2.66974248	-1.03775814
C	1.26344601	2.65232254	0.60419842
H	2.25944598	2.66989214	1.03778117
C	0.62606359	3.87647261	0.30428469
H	1.12970910	4.81466137	

		0.54027777	
C	4.90847604	0.76722825	1.10545265
H	4.89366865	0.83478664	2.19382216
C	-0.62638512	3.87642990	-0.30420417
H	-1.13012210	4.81458654	-0.5401433
C	6.11916784	0.95145525	-0.98587729
H	7.03838995	1.15681983	-1.53341501
C	-4.90848310	0.76716615	-1.10546556
H	-4.89368364	0.83474653	-2.19382891
C	-3.76425001	0.35009902	0.97007659
H	-2.84542575	0.08646974	1.4867186
C	6.09483453	1.02780803	0.41145897
H	6.99816195	1.29491893	0.96023286
C	- 4.94503885	0.61191789	1.67007837
H	-4.94952913	0.55156832	2.75770556
C	-6.09482251	1.02775026	-0.41145425
H	-6.99815178	1.29490946	-0.96020321
C	-6.11914757	0.95136376	0.98588786
H	-7.03836518	1.15674554	1.53342364

S3			
Pd	0.00034872	-1.32463997	0.00003284
Cl	1.49006611	-2.99780189	0.79929994
Cl	-1.48817317	-2.99887053	-0.79926143
N	1.15705107	0.24896382	0.62573196
N	-1.15739652	0.24820321	-0.62580143
C	-0.64527912	1.45946118	-0.3410423
C	3.66358031	0.37237519	0.50462649
C	3.81660244	-0.26254586	-0.73797005
H	3.02254382	-0.90756122	-1.10207724
C	0.64436245	1.45989061	0.3405454
C	-3.66391956	0.37122768	-0.50433313
C	2.41794997	0.13625130	1.3499268
H	2.45769862	-0.88204657	1.74729298
H	2.42294523	0.82741271	2.20663757
C	-2.41840780	0.13464559	-1.34966843
H	-2.42373006	0.82511451	-2.20696421
H	-2.45798308	-0.88397634	-1.74621194
C	4.98036626	-0.08122941	-1.48839591
H	5.08271692	-0.58363234	-

	2.44789177		1.48925636
C	-1.25445435	2.71249329	-
	0.64819365		2.44916301
H	-2.22851737	2.73038425	-
	1.12235628		0.22794828
C	1.25290071	2.71331776	
	0.64731529		0.61192309
H	2.22693195	2.73185712	
	1.12153858		1.01135454
C	0.62816600	3.90544959	
	0.32263163		1.59902041
H	1.11334504	4.84914467	
	0.56244021		S4
C	4.70524774	1.18303922	
	0.97523732		0.00001245
H	4.60154161	1.68053252	
	1.93890243		0.84378268
C	-0.63030239	3.90503432	-
	0.32390057		0.84364035
H	-1.11594659	4.84841591	-
	0.56400406		0.66319249
C	6.01457892	0.73279623	-
	1.01097234		0.66324777
H	6.91963829	0.87209470	-
	1.598573		0.36870874
C	-4.70579642	1.18132139	-
	0.97540035		0.53234459
H	-4.60232604	1.67806257	-
	1.93948223		0.60504281
C	-3.81664169	-0.26276874	
	0.73879472		0.86887205
H	-3.02244750	-0.90743694	
	1.10323807		0.36866726
C	5.87452174	1.36374229	
	0.22783157		0.53239931
H	6.66950435	2.00044497	
	0.61140091		1.40379342
C	-4.98029344	-0.08104883	

H	-5.08242944	-0.58270991	
	2.44916301		
C	-5.87500784	1.36242249	-
	0.22794828		
H	-6.67015820	1.99867359	-
	0.61192309		
C	-6.01474334	0.73244067	
	1.01135454		
H	-6.91971417	0.87203079	
	1.59902041		
	S4		
Pd	0.00002986	-1.30873894	-
	0.00001245		
Cl	1.40504552	-2.95616608	
	0.84378268		
Cl	-1.40492933	-2.95628444	-
	0.84364035		
N	1.13912509	0.27768458	
	0.66319249		
N	-1.13911841	0.27763933	-
	0.66324777		
C	-0.64474885	1.45703183	-
	0.36870874		
C	3.64010947	0.34873185	
	0.53234459		
C	3.85554387	-0.44481671	-
	0.60504281		
H	3.13546799	-1.21360670	-
	0.86887205		
C	0.64471021	1.45705482	
	0.36866726		
C	-3.64010549	0.34868781	-
	0.53239931		
C	2.40939427	0.14113755	
	1.40379342		
H	2.40913324	-0.87191527	

		1.81033502	
H	2.41558229	0.84573558	-
		2.24332289	
C	-2.40939158	0.14105587	-
		1.4038381	
H	-2.41558662	0.84560668	-
		2.24341648	
H	-2.40912087	-0.87201192	-
		1.81034181	
C	5.00444467	-0.26740091	-
		1.37904318	
H	5.16056632	-0.89077517	-
		2.25565675	
C	-1.24965131	2.73141123	-
		0.69915071	
H	-2.20462294	2.75182445	-
		1.20636217	
C	1.24951253	2.73148023	
		0.69916043	
H	2.20452453	2.75197186	
		1.20627686	
C	0.63149921	3.89150018	
		0.35041562	
H	1.09249485	4.84378904	
		0.59723212	
C	4.60168307	1.30470189	
		0.88604901	
H	4.46037922	1.91058928	
		1.77986119	
C	-0.63180713	3.89147184	-
		0.35024336	
H	-1.09291220	4.84373722	-
		0.59695303	
C	5.95676541	0.69393689	-
		1.02391334	
H	6.85192868	0.82532667	-
		1.62629256	
C	-4.60177845	1.30454152	-
		0.88618794	
H	-4.46055201	1.91031339	-
		1.78006951	
C	-3.85545555	-0.44476298	
		0.60505794	
H	-3.13534572	-1.21351426	
		0.86893973	
C	5.75634222	1.47649342	
		0.11564899	
H	6.49589548	2.21746265	
		0.4087052	
C	-5.00436050	-0.26737272	
		1.37908473	
H	-5.16038380	-0.89070082	
		2.25574776	
C	-5.75641890	1.47630390	-
		0.11578212	
H	-6.49606423	2.21717065	-
		0.40886971	
C	-5.95675901	0.69383668	
		1.02387743	
H	-6.85194831	0.82523412	
		1.62621466	
S5			
Pd	0.00036851	-0.01834628	-
		1.06985361	
Cl	1.65604193	-0.74511830	-
		2.53321694	
Cl	-1.65425910	-0.74616079	-
		2.53397861	
N	1.31969046	0.98168178	
		0.26962667	
N	-1.32001500	0.98156642	
		0.26931217	
C	-0.70703389	2.26381734	
		0.390972	
C	3.14590799	-0.52183568	

		1.01557689	
C	2.68284161	-1.75903830	0.52666068
H	1.73787184	-1.81398016	0.0012729
C	0.70649920	2.26383592	0.39132208
C	-3.14657669	-0.52185882	1.01481527
C	2.40689037	0.72926877	0.92210162
H	2.82468171	1.54298085	1.52355082
C	-2.40754392	0.72924577	0.92128137
H	-2.82553231	1.54293835	1.52261308
C	3.45047551	-2.90708504	0.70159418
H	3.08840830	-3.85487212	0.31363265
C	-1.40299348	3.47236370	0.47177898
H	-2.48742410	3.47816786	0.41598396
C	1.40247458	3.47234902	0.47250748
H	2.48693387	3.47806888	0.41725112
C	0.69827816	4.67672893	0.56228894
H	1.24394455	5.61517461	0.59914095
C	4.38261972	-0.47296188	1.69372707
H	4.74149688	0.47667922	2.08527491
C	-0.69880667	4.67672285	0.56189995
H	-1.24448977	5.61517133	0.59845159
C	4.68488345	-2.84329613	1.35945928
H	5.28004003	-3.74408970	1.48537206
C	-2.68334467	-1.75928207	0.52659368
H	-1.73825903	-1.81445213	0.00148708
C	-4.38351127	-0.47274978	1.69256591
H	-4.74254016	0.47704713	2.08359475
C	5.15211794	-1.62223249	1.85699907
H	6.10765289	-1.56832219	2.3711593
C	-5.15304048	-1.62195354	1.85608942
H	-6.10871971	-1.56784018	2.36995908
C	-3.45104195	-2.90725340	0.70172106
H	-3.08886059	-3.85518506	0.31421395
C	-4.68565454	-2.84321590	1.35917628
H	-5.28083769	-3.74396668	1.48527338